Fermi National Accelerator Laboratory

FERMILAB-FN-601

SSCSIM: Development and Use by the Fermilab SDC Group

A. Beretvas, K. Denisenko, D. Green, J. Marraffino, A. Para and W. Wu

Fermi National Accelerator Laboratory
P.O. Box 500, Batavia, Illinois 60510

February 1993

Operated by Universities Research Association Inc. under Contract No. DE-AC02-76CHO3000 with the United States Department of Energy

Disclaimer

This report was prepared as an account of work sponsored by an agency of the United States Government. Neither the United States Government nor any agency thereof, nor any of their employees, makes any warranty, express or implied, or assumes any legal liability or responsibility for the accuracy, completeness, or usefulness of any information, apparatus, product, or process disclosed, or represents that its use would not infringe privately owned rights. Reference herein to any specific commercial product, process, or service by trade name, trademark, manufacturer, or otherwise, does not necessarily constitute or imply its endorsement, recommendation, or favoring by the United States Government or any agency thereof. The views and opinions of authors expressed herein do not necessarily state or reflect those of the United States Government or any agency thereof.

SSCSIM: Development and Use by the Fermilab SDC Group

A. Beretvas, K. Denisenko, D. Green, J. Marraffino, A. Para, W. Wu

To be submitted to the International Conference on Monte Carlo
in High Energy Physics and Nuclear Physics (1993)

Presented by Weimin Wu

Introduction

Since 1990, the Fermilab SDC group has developed a simulation program, SSCSIM, for the proposed detector at the SSC. The main authors are A.Beretvas, D.Green, A.Para and W.Wu. R. Bernstein, N. Denisenko, K. Denisenko and H. Iso, were also involved in the program development. The motivation for developing this program was to investigate various aspects of the conceptual design for the calorimeter for SDC, both for the Letter of Intent (LoI), and the formal Technical Design Report (TDR). The program was intended to be a tool for a reasonably complete investigation of questions involving the relations between the detector parameters and the physics capabilities of the detector.

The prototype of the program was completed in early 1990, with input data in ISAJET format. A major modification was started in later 1990 to use the international HEP format for input data, allowing the program to use most of the available event generators in High Energy Physics. Actually, the interface between the ISAJET and the HEP format was developed by the FNAL group.

Since 1991, as more details of the physics requirements for the calorimeter design were needed for SDC, more features were incorporated into SSCSIM, including jet finding and the clustering methods. Now SSCSIM includes 66 subroutines and needs 58 data items to specify all options and parameters. In addition, there are many default values which also could be part of selected options by users.

SSCSIM is written in standard FORTRAN 77. It has been installed and used under the VMS operating system, mainly on the Fermilab Physics Department vax cluster at Fermilab. It also could be installed and used on the SUN workstation under the UNIX system.

Reviewing the results we have produced using SSCSIM during last 2-3 years, we conclude that the initial goal of this program has been achieved. This paper is a summary of the program to date.

Program Structure and Users Guide

The consequences of various technological choices and tradeoffs between conflicting requirements for the physics potential of SSC experiments must be carefully examined. Most of these questions can be answered with a simplified model of the detector, since many of them are of purely kinematical or geometrical character. At this stage it is possible to address these questions without resorting to very complicated, usually very slow, and incomprehensible large packages like GEANT. At an early design stage, one only needs a simple framework which provides an interface between the event generators, detector simulation and the analysis code. This enables one to propagate particles generated by standard event generators through the detector, simulating various detector-specific effects. Some simple examples of physics analysis are provided as a possible template.

The structure of the program is shown in Appendix A. After initialization, the requested number of events is read from the user specified data files. If requested, background events from a separate file can be overlayed on a "signal" event. The particles produced by the event generator program are traced, optionally through a uniform axial magnetic field, to the inner surface of the calorimeter. At present, only the simulation of the calorimeter part of the detector is implemented. Extensions to simulate other elements of the detector are straightforward. This would be accomplished by using information about the kinematics of all particles as extracted from the HEPEVT common block.

The detector is modeled as a solenoid of half-length HALFLE and radius RADCYL with a uniform magnetic field BFIE. The central detector, referred to as the barrel, is supplemented by endcaps that extend to ETAMAX. The detector response is assumed to be in the form of energy deposition in projective towers with dimension DETA * DPHI. Longitudinal segmentation is provided.

A flow-chart of the program is shown in Appendix B. An example of user data cards and the job execution script is shown in Appendix C.

The capabilities of SSCSIM can be seen from the user input data and its explanation. These can be controlled by selecting proper data items to run any given job.

1. The number of events to be simulated can be chosen by users as well as the number of overlap events (background, minbias, etc). That number refers to the mean of a Poisson distribution.

2. Users can indicate which parton in the physics process produced by the event generator is wanted for study, so that only particles from the fragmentation of the indicated parton will be propagated.

3. The program can be used to analyze jets, or to study the detection of charged leptons in the shower-max strips.

4. Users can choose to use a jet finding method to reconstruct jets, or use the original parton direction to define a jet.

5. Users can choose to deflect particles in the magnetic field with given strength. The field is assumed to have solenoidal geometry. The intersection of helices with the inner surface of the calorimeter, for both the barrel or endcap parts, is calculated analytically.

6. The energy deposited by the particle is distributed in space around the initial direction. For electromagnetic showers a Gaussian distribution with 1 cm width is assumed. For hadron induced showers a convolution of two Gaussians is used, with parameters taken from F. Binon et al., NIM 206 (1983), 373. However, the parameters of the profile are subject to change by the user.

7. The energy of the incoming hadrons, electrons and photons may be smeared using the formula E' = E inc * (1 + dE/E), where dE/E is distributed as a Gaussian with $\sigma^2 = \left(a/\sqrt{E}\right)^2 + b^2$. Stochastic and constant terms in the resolution function are different for hadrons and electromagnetic particles.

8. Non-linearity of the response of the hadron calorimeter (or deviation of e/h from 1.00) is simulated using the prescription of D. Groom, SSC-227. The parameters in Groom's formula can be modified by the user.

9. There are two sections of the calorimeter: the hadronic section and the electromagnetic section. Users can define the length for both of them, and also may choose between Fe or Pb for the hadronic section. The EM section is fixed with lead assumed to be the absorbing material.

10. The transverse segmentation of the hadron calorimeter may be chosen by the user. The cell size for the EM section can be chosen as either equal to that for the hadronic section, or equal to half the cell size of the hadronic section.

11. Users are allowed to choose the η and ϕ coverage. SSCSIM can be used with η coverage extended to the endcap part or not. Very large η coverage does require correspondingly large amounts of memory, especially with very fine granularity.

12. Users are allowed to select the size of the calorimeter by defining the length and the radius of the barrel section

13. The primary vertex position can be smeared both in the barrel part and in the endcap part, by defining $d\phi$ with dZ or dR.

14. SSCSIM has special flags to tag Z pairs, W pairs, or one W only.

15. Random noise may be added in each cell. It is parameterized with a Gaussian distribution of user selected width in energy. Users may also choose the noise discrimination threshold for each tower.

16. SSCSIM has a simple model to simulate the effect of "cracks" between towers. The calorimeter is assumed to be made up of 32 modules placed at a constant radius. The user may select a non-zero spatial separation between the modules. Other sorts of arrangements are possible.

17. SSCSIM has used the EGS program to simulate the EM energy response loss due to radiation damage by a given radiation dose. Users may choose to include this effect for the EM calorimeter.

18. SSCSIM has options to select some thresholds, such as initial and final lepton Pt in a decay chain, and the ratio of EM energy over the HAD energy in the given lepton direction. These options are useful for lepton isolation studies.

19. SSCSIM has options to select multiple cone sizes (used by the jet finding code). This is very useful for jet studies.

20. SSCSIM has options to select the logical unit to which the user wants various output files directed. This includes things like summaries and histograms. The corresponding histogram files are written in an area indicated by the user in the job execution command.

As one can see, SSCSIM has quite powerful capabilities for studying various topics related to calorimeter conceptional design.

Main Results

A number of specific physics topics were chosen for study in order to explore the physics capabilities with different detector parameters. Such studies were crucial to the calorimeter conceptual design for SDC.

We summarize the main results in what follows, and highlight the most important conclusions without mentioning the details which have been described in the indicated references.

1. Top Quark Mass Measurement in Very High Pt (2-8 TeV/c)

A file of top quark events was produced where the t was produced with very high Pt, averaging 2.3 TeV/c, with subsequent decays into b and W. The motivation was to examine what kind of granularity is sufficient to reconstruct highly boosted top and what impact that may have on other major detector components. The main results are given in Table 1.

Table 1 indicates that a granularity of 0.05 is fairly good without losing significant mass resolution since, with a cone size of 0.5, the corresponding mass resolution is 10.7%.

If we include other major detector effects, the above results for a fixed cone size R at 0.5 and the granularity fixed at 0.05 are shown Table 2. Thus, with default parameters, the mass resolution for the "real" detector compared to an "ideal" detector is degraded by only 13%. Therefore, the mass resolution is dominated by the physics itself. This is the first result of SSCSIM which was obtained shortly after the prototype was brought into operation in early 1990 [1].

2. Z Study (LoI): Jet Energy Resolution in a "Real" Detector

The SSC Program Advisory Committee had asked a question: "Demonstrate the jet energy resolution of your proposed detector by studing decays Z-->jet+ jet, and Z'--> jet + jet, for a Z' of mass of 1 TeV."

For that study, we produced an ISAJET output file for Drell-Yan Z production, with low Pt (50-60 GeV/c), high Pt (500-600 GeV/c) and with Z masses at around 100 and 1000 GeV.

Our tentative conclusion from this study is that physics induced effects, out-of-cone fluctuations and underlying event fluctuations, dominate the resolution. Pushing the detector perfomance to the limits of technology improves the effective resolution by at most 20% [2].

In the case of lower Pt Z's, the mass resolution is dominated by the fluctuation of energy outside the 0.7 cone and fluctuations in the underlying event.

For high Pt Z's, all particles are well contained in the cone. There is not much to be gained by pushing detector perfomance to the limits of technology. This conclusion agrees with previous high Pt Top mass resolution studies.

Fig. 1 shows the summary results. From point "a" to point "b" is detector independent; the effect of any resonable HAD calorimeter resolution is minimal.

3. Jet Fragmentation

CDF has already published some jet fragmentation functions [3]. It is interesting to compare ISAJET jet fragmentation with real data. We have used SSCSIM to do that and found agreement between the CDF experimental data and the result produced by ISAJET/SSCSIM, which is shown in Fig. 2.

4. Hadronic and Electromagnetic Transverse Calorimetric Segmentation

In a calorimeter system, one of the major cost drivers is the number of towers. The transverse segmentation of the system necessarily mirrors the characteristic size of the shower process: the Moliere radius for the electromagnetic (EM) compartment and the absorption length for the hadronic (HAD) compartment.

The kinematics of dijets, ignoring fragmentation, implies that the mass resolution, dM, for a dijet of mass M due to an angular error $d\theta$ is given by

$$dM/M = d(\theta)\,[Pt/M] \qquad (1)$$

This leads us to expect that only highly boosted, light dijets will have a significant contribution due to any angular error in comparison to the energy error due to the calorimeter measurement. This expectation is borne out in Fig. 3. Only the highly boosted Z shows a substantial effect due to segmentation [4].

However, our study also shows that the hadron compartment (HAD) segmentation does not effect dijet masses, even when the jets are highly boosted if the HAD segmentation is < 0.1. This occurs because of the basic limitation on jet measurement due to hadronic shower size which is around 0.075 in the SDC geometry. Confirmation of this expectation is shown in Fig. 4 which shows Z dijet masses for EM segmentation of 0.05 and HAD segmentation of 0.05 and 0.1.

For studying EM segmentation, it was decided to look at a process which yields electrons near jets. Top quark pairs with a top mass of 150 GeV and over a very wide Pt region (between 2 GeV/c and 8000 GeV/c) were generated. The decay mode was Top decays into W and b, and the W was unconstrained while the b quark was forced to decay semileptonically into c, e and neutrino. No cut on Pt of the lepton with respect to the c jet

axis was made. Therefore, the electrons which are studied are not forced to be isolated. Hence, this sample is deemed to be representive of the difficult category of electrons which are not well isolated.

Fixing the EM segmentation at 0.05, one can ask what effect the HAD segmentation has on the EM/HAD ratio. In Fig. 5, we show the functional dependence of the EM/HAD ratio on the radius of a cone, defined to be

$$R = \sqrt{(\Delta\eta)^2 + (\Delta\phi)^2} \tag{2}$$

centered on the EM centroid tower.

Clearly, the coarser HAD segmentation leads to a reduction in the EM/HAD ratio. The reduction of the ratio is quite small as HAD segmentation goes from 0.05 to 0.1. A typical LEGO plot for EM plus HAD is shown in Fig. 6 for pixel sizes of 0.05. It seems that, even in the nonisolated environment chosen, a small HAD segmentation is not crucial to obtaining a large value of EM/HAD. Of course, smaller EM segmentation at the size of the natural scale of electron showers is not economically feasible. With EM (HAD) segmentation of 0.05 (0.1), within R = 0.05 (about 1 HAD tower), a cut of EM/HAD > 30 is efficient for this process.

A segmentation which yields acceptable performance at design luminosity may degrade at a luminosity 10 times higher. To study pileup effects, minimum bias events were overlayed on the top events. Typical LEGO plots, with and without B field, are shown in Fig. 7 and Fig. 8. Direct comparison with Fig. 6 allows one to get some idea as to the severity of the pileup problem. The pileup effect clearly increases with R. At R = 0.1, the pileup reduction in the EM/HAD ratio is about 30%. The conclusion derived from this study was that 0.1 HAD segmentation does not lead to unacceptable pileup effects for this physics process. However, effects do appear for large cone sizes, R > 0.1.

5. Depth Requirements in SSC Calorimetry

The depth requirement is a crucial cost driving element as it defines the size of the muon system, and the materials cost of the calorimeter itself. For this reason, it is imperative to make the calorimeter depth as shallow as possible. Balancing this tendency, the depth must be of a sufficient thickness so as not to compromise a variety of physics issues such as the filtering of hadrons before they enter the muon system.

The first task to be accomplished is to collect data on longitudinal leakage and leakage fluctuations in calorimeters. This data could be parameterized and that parameterization used in a Monte Carlo program. It was thought to be important to use an ensemble of data sets since they would differ in energy range, beam tagging, transverse containment, longitudinal containment, and perhaps other systematic factors. It is also true that in extrapolating to the SSC, one must go beyond the region of validity of the data. A variety of functional fits allows one some idea of the systematic errors in this case.

We have used CITF, WA1, CDHS and LAB E data as our models [5]. The spread among them is an indication of the "systematic error" to be found among the existing published data on depth and energy resolution in hadron calorimeters.

The question is what is the highest possible dijet mass which can be measured at SSC design luminosity with a given depth of the calorimeter? In order to answer this question,

the physics process chosen was dijet events at the highest accessible (rate limited) mass, M = 10 TeV.

We have shown the standard deviation of the reconstructed to generated dijet mass ratio as a function of cone radius. When the underlying event and its fluctuation are added, the minimum error occurs at R = 0.6. A typical histogram of the ratio of reconstructed to generated dijet mass is shown in Fig. 9. Note the long "radiative" tail, due to gluon radiation and neutrinos. Fig. 10 shows the histogram of the fraction of the jet energy carried away by neutrinos. The result for the mass error as a function of calorimeter depth is shown in Fig. 11. A plot of the ratio of the mean leakage energy to the mean neutrino energy for 10 TeV dijets is shown in Fig. 12 as a function of calorimeter depth. At a depth of about 12 absorption lengths, the leakage energy falls below the "intrinsic" leakage due to neutrinos from heavy flavor decays.

Our study also shows that real muons dominate over punchthroughs for a calorimeter thickness > 7 absorption length. Since this thickness is less than that which has already been considered on the basis of resolution and leakage studies, which is about 10 absorption lengths, one concludes that no more stringent requirement appears to be imposed by consideration of the muon system. The dijet mass resolution, dM/M, is about 2% for depth > 10 interaction lengths.

Until now the calorimeter has been considered to be a unitary object. In the WA1 model, dividing a D = 10 calorimeter into D1 = 6 and D2 = 4 segments allows one to estimate and/or tag the leakage. SSCSIM provides a parametrization of the average longitudinal development which allows one to roughly estimate leakage.

It was found that no improvment in the Gaussian part of the resolution could be obtained using information from the two depth segments. However, it is extremely useful in vetoing the long tail in the resolution corresponding to poor containment and large leakage.

In conclusion, given a systematic error spread due to the extrapolation of existing data, a calorimeter with depth D = 10 segmented into D1 = 6.5, D2 = 3.5 will not degrade the jet measurement, the muon system performance, or the missing transverse momentum measurement at the SSC.

6. Energy Resolution and Radiation Damage

We have studied the hadronic energy resolution related to the radiation damage [6] to connect the radiation dose, by way of the "damage" profile, to the physical quantities in question which define the performance of the calorimeter system. We will mention this study later. Here, we just mention how the radiation damage impacts the jet energy resolution using SSCSIM.

As we know, radiation dose can damage the sensitive material of the calorimeter. As a result, the response to light will be degraded and therefore the energy resolution will be also degraded due to this effect.

We have simulated the energy response as a function of the energy for different radiation doses, characterized by the value d, the peak damage factor, [6] using the EGS program. See Fig. 13. Now the question is how much jet energy resolution will be lost corresponding to that damage? We used the file of dijet of Z's at mass of 0.1, 1.0 and 10 TeV, and only consider the gammas and electrons which reduced their measured energy by an amount which was interpolated by a polynominal of third order in Fig. 13. Obviously,

the E/E0 = 1 means that there is no radiation damage. The results are in Table 3. One can see that the energy resolution can worsen by a factor of up to 5 for increasing radiation dose levels [7].

7. Compensation in Calorimeter

The SDC has decided to build a scintillating Tile/Fiber calorimeter. The SDC calorimeter will contain a 22 radiation length (X_0) EM compartment. The EM calorimeter will consist of 36 pairs of plates. This calorimeter has a total thickness of 0.7 nuclear interaction lengths. Two options (lead/scintillator or iron/scintillator) were considered for the hadron (HAD) calorimeter. For both options the total thickness is 8.3 λ, as shown in the depth study, which made the total depth of calorimeter of 9 λ.

Our study finds that the mass resolution is essentially the same in both cases and the energy resolution for lead is only slightly better than for iron, 1.9% versus 2.2% for $Z' \rightarrow$ jet + jet at MZ' = 10 TeV [8].

The first step is to make an EM and HAD shower longitudinal and transverse parametrization. With that, we can determine the fraction of the EM and HAD shower energy deposited in the EM calorimeter and the HAD calorimeter respectively. EM energy will be deposited mostly in the EM compartment, but still will have some leakage into the HAD compartment, and the HAD energy will be mostly deposited into the HAD compartment, although there will be hadrons which interact in the EM compartment. The energy resolution of the calorimeter is approximated by a "stochastic" term due to statistical fluctuations in the shower/detection process and a "constant" term due to non-uniformities in the detector.

The deposited energy for hadrons is specified by the ratio of e/h. We have used the Groom formula to do this, and an additional constant term needs to be added in quadrature due to the smearing. We introduced this strategy into SSCSIM, and applied it to the Z mass resolution study. We used the e/h value of 1 for lead, and 1.25 for iron. The summary results are in Table 4. Clearly, no major differences in the response of an iron and lead calorimeter are observed. Subsequent data taken with a test beam have strongly supported the conclusions of this study [9].

8. Shower-max Strips and Length

A shower-max detector aids substantially in the identification of electrons and photons by measuring the shape and location of the EM shower. It is composed of crossed strips of scintillators and is located near the shower-maximum point. The first issue is to demonstrate the necessity of the shower-max device.

We have looked at Higgs (800) [10] decays into two Z0's where one of Z0 decays into τ pair, one τ decays into ρ and ν, then the ρ decays into a π^0 and charged a π. The π^0 then decays into two γ. In order to identify this process, two photons must be resolved. Since the opening angle between the two gammas has an average of 0.013 radians, (see Fig. 14) the shower-max strip detector is essential as can be seen in Fig. 15.1 - 15.2.

The same top events which were used for the EM segmentation study were used again in a study of shower-maximum (SM), especially to examine the question of how long the SM strips may be made for the identification of the electrons from the decay sequence of $t \rightarrow b \rightarrow e$.

The detector was taken to have crossed strips of width = 0.05/8 = 0.00625 in η and ϕ. For a radius of 2 m, this corresponds to a physical size of 1.25 cm. This size is comparable to the Moliere radius in Pb. We modified the LEGO plots to be asymmetric. The tracking centroid was taken to be the point of impact of the electron trajectory on the front face of the EM calorimeter compartment. The SM centroid was taken to be the energy weighted center of gravity of the three strips nearest the impact point. The electron energy was distributed transversly according to a two component exponential parametrization which attempts to model a hot core and the cool low energy shower components [11].

The results for the SM/track match for both "η" and "ϕ" strips are shown in Fig. 16. The mean deviation of the match as a function of the strip length is shown. No pileup is applied for the solid curves, while a mean of 15 minbias events is overlapped with the $t\bar{t}$ events for the dashed curves.

Ideally, the SM strips would be the same length as the EM towers (0.05). However, given the existing financial constraints, we can not make the length too short. Our results show that for strip length < 0.2, the pileup fluctuations at low and high luminosity are less than 1 mm (about 0.0005). Note also that high luminosity operation makes little impact on the SM performance for strip length < 0.2. The mean deviation of the match of SM/tracking is rather weakly dependent on the SM strip length.

9. Missing Energy Resolution, Cracks and the Forward Calorimetry

The importance of the forward detector ($3.0 < |\eta| < 6.0$) and the impact of the cracks were studied using SSCSIM. The process we have chosen to investigate is Higgs (800) decay as we have mentioned before. [10]

The signature for these events will be a "boosted" Z. This high Pt Z will then appear as either two jets from q and $\bar{q}$, or as high Pt π^0 and charged πs forming two low mass ρ clusters along with a large transverse missing Pt from the two neutrinos. The reconstuction of π^0 from the two γ needs SM as mentioned above. The transverse neutrino energy is determined in the standard way by summing the energy in the LEGO plots:

$$\text{Et (neutrino)} = \sqrt{(\text{Ex(neutrino)}**2 + \text{Ey(neutrino)}**2)}$$

$$\text{Ex (neutrino)} = -\sum (\text{ENERGY}(\eta, \phi) * \text{SIN}(\theta) * \text{COS}(\phi))$$

$$\text{Ey (neutrino)} = -\sum (\text{ENERGY}(\eta, \phi) * \text{SIN}(\theta) * \text{SIN}(\phi)) \qquad (3)$$

We have investigated the major impacts on the missing energy resolution, which includes the angular range of the detector (η limits), the hermiticity (cracks), the noise and threshold, granularity of EM and HAD cells, e/h, and the number of overlapped minimum bias events. Summary results are in Table 5.

The conclusion is that η coverage out to $\eta = 5$ is necessary for good missing Pt resolution. The Zt fractional mass resolution is degraded from 16.0% to 22.9% due to shower-max cell size, and 14.2% to 21.4% due to EM calorimeter resolution. The cracks, corresponding to 8.8% of the energy being lost, appear to have only slightly worsened the Z transverse mass resolution, because other detector effects conceal the problems due to the cracks. A very small cell size will not help the transverse missing energy resolution, because the noise and threshold effects are assumed to be per cell and thus make a much larger contribution by accumulation from many more small cells. High luminosity does slightly degrade the resolution, degrading the Zt mass resolution by about 3%, as compared to about 6 % due to the incomplete η coverage.

10. Higgs (80-125 GeV) into 2 γ Search and EM Calorimeter Resolution

A light Higgs (mass of Higgs < 85 GeV) will almost certainly be found at LEP II before the SSC turns on, while a heavy Higgs (mass of Higgs > 180 GeV) will be studied using Z^0Z^0 pairs. The intermediate mass Higgs seems to be problematical. There is a strong claim [12] that the detector with a "conventional" resolution will not be able to do Higgs into 2 γ physics in the Higgs mass region of 80 - 160 GeV. The motivation of our study is to understand how bad is bad.

We have produced 5000 Higgs (80) and Higgs (125) which decay into two gammas events, and the file of "irreducible" background ($q\bar{q}$) into two γ which contains 100,000 events from the ISAJET. We used the same program SSCSIM using the clustering method to find the gammas jets from the signal and the background in the EM calorimeter. We used the background mass distribution of 100,000 events to determine the shape of the background. A smooth, statistically correct background distribution is then generated for a one year SSC run, namely up to one million background events. The fluctuation of the background is reduced down to 0.3% level, which is necessary to match the ratio of the signal/background which is around 0.3 - 0.5%. The same program and algorithm have been used for signal and background.

As we know, the mass resolution for reconstructed two photon events can be expressed as:

$$\frac{dM}{M} = \frac{1}{2}\sqrt{\left(\frac{dE_1}{E_1}\right)^2 + \left(\frac{dE_2}{E_2}\right)^2 + \left(\cot\left(\frac{\theta}{2}\right)d\theta\right)^2} \tag{4}$$

$$\frac{\Delta E_i}{E_i} = \frac{a}{\sqrt{E_i}} \oplus b \tag{5}$$

We took "a" equals 0.02, "b" equals 0.002 as "super" resolution, and "a" equals 0.2, "b" equals 0.02 as "conventional" resolution. Our study shows [13], [14] that the angular resolution will significantly contribute to the mass resolution for the "super" energy resolution calorimeter, so it is very crucial to determine the correct vertex and measure the photon directions. This can be obtained by using shower-max, or some sort of built-in position detectors. We took 0.001 radians for PHI resolution and 0.25 cm for sigma in both r and z directions. The final Higgs mass resolution in our study includes the effects of

both the angle and vertex measurement for both types of EM calorimeter. If the "super" energy resolution calorimeter does not have the built-in position detector due to mechanical or technical reason, the mass resolution could be even worse.

The comparison of the perfomance of the "super-resolution" calorimeter and the "conventional resolution" calorimeter on this physics topic has been made in this study. The summary results are in Table 6. We can see that the ratio of the Higgs mass resolution for different energy resolution calorimeter is 2.15 times for the Higgs mass at 80 GeV, and 1.92 times for the Higgs mass at 125 GeV. Final plots are shown in Fig.17 [13], [14], [15].

A similar study was done a few years ago[16]. We note that they choose to determine the shape of the background using a small sample (5000) of PYTHIA events, compared to our 100,000 samples.

Jet Finding and Clustering Method

We have developed an algorithm based on clustering methods for jet finding within SSCSIM [17], [18]. Separately, SDC is developing a program, SHELL, as its initial software for the detector, which needs a jet finding program using the clustering method for the calorimeter. We have modified our clustering program as an independent package and installed it into the SHELL, and sucessfully tested it there [19].

The clustering package is divided into three parts. The first part is an initialization; the second part is to find and report jet candidates. We emphasize that this process depends only on the energy map (raw data) and nothing else. The information reported by the program includes: the number of jets found above the given threshold, the 4 vectors for each jet, and the number of towers struck by the jet. The user then has this information available for further analysis. The third part provides a general reconstruction program that can be used to compute things like the invariant mass of the dijets or the highly boosted single jet mass.

Fig. 18.1-18.5 show the comparison of the dijet mass for low P_T (55 GeV/c) and high P_T (550 GeV/c) at Z' mass of 100 GeV, 1000 GeV, and 10 TeV. The dijet reconstructed mass using the "quark" method is given by a solid line and using the clustering method by a dashed line. This program package is quite mass independent.

Other Calorimetry Studies Done by the Fermilab SDC Group

The Fermilab SDC software group is also engaged in many other activities apart from using SSCSIM. We will not go into detail in this paper other than to briefly mention a few main points. Typically, EM showers are simulated using EGS and hadronic shower study using experimental data [9].

1. "Massless Gaps" for SDC Calorimeter

The necessary existence of material in front of the first active element in a calorimeter will degrade the performance of that device. The question is by what factor? The follow up question is what can be done to minimize the damage.

To examine this question, the array which was put into EGS4 was a stack consisting of Al, 10.68 cm thick representing the magnet coil, followed by pairs of 2.5 mm thick scintillator plates and 3.175 mm thick Pb plates repeated 50 times. This stack is about 25 X0 thick which will allow a study of the exit leakage fluctuations. The appropriate vacuum space between the solenoid coil and the first active element of the EM stack has been defined. The data set consists of 12.5, 25.0, 50.0 and 100 GeV incident electrons at 30 and 90 degree incident angles. Our study shows that a first element weight of 1.75 (Fig. 19) can be chosen independent of angle and energy. That choice leads to a resolution which does not degrade the resolution expected for SDC EM calorimetry. The induced nonlinearity due to this weighting procedure is not comparable to the intrinsic energy resolution of the SDC EM calorimetry. Therefore, the adoption of the simplest possible massless gap scheme is sufficient for the purposes of maintaining the resolution made available by fine grained (about 0.5 X0) sampling [20].

Similar studies have been done for 3.175 mm thick Pb plate [21], and for the limits of the thickness of the upstream materials [22]. Our study shows that the energy resolution for 1.2 X_0 of inserted materials is still within errors compared to the 1.0 X_0 using a weighting strategy, but for 1.5 X_0, the resolution will be 30% larger than the case of 1.0 X_0 even with a weighting strategy.

2. A Weighting Strategy for Compensating Leakage in the SDC Electromagnetic Calorimeter

Economic constraints, among others, impose a real limit on the depth of any calorimeter. But, the effect of energy leakage due to the finite length of the calorimeter on the resolution can be compensated by weighting the last three layers of readout. Our study shows that it is possible to nearly recover the energy resolution by this strategy with acceptable nonlinearity [23]. The energy and the shower angle dependence of the weight factor are obtained. In addition, we also used this strategy for the extreme case of a completely dead channel at shower-maximum to study the effect of a dead channel. In this case, the total energy deposit is reduced by about 6% and the resolution is worsened by about 18%, which is nearly energy and angle independent.

3. Radiation Damage and Hadronic Resolution

In order to make a model of the damage, we use 15 GeV energy deposition data from Lab E [24]. The longitudinal energy deposition profile, f(z), was normalized to unity integrated over all z. A weight was defined according to $WT(z)= 1 - g*f(z)$. Typically, for $g = 1$, the minimum value of the weight was around 0.8. A plot of WT(z) for $g = 1$ is shown in Fig. 20. Note that each layer, except the first, is 0.7 absorption length thick. Thus, the hadronic shower maximum for 15 GeV incident pions occurs at a depth 1.5 absorption lengths. We further assume that the damage is local, so that the response is proportional to the weight. This assumption has proved to be valid in the case of EM radiation damage. For EM doses and the standard SDC plastics, a dose of 1 Mrad would lead to a peak damage factor of $\bar{d} = 0.28$ or $WT = 0.72$.

Having made a model of the induced nonuniformity of the detecting medium, one can continue and find the effect on performance of the detector. To that end, data [24] from hadronic showers was weighted in each layer by WT(z) for different assumed peak damage, $\bar{d}$, due to radiation doses. Incident energies of 50, 100, 200 and 450 GeV were used. To characterize the response of the nonuniform detector, fractional induced

nonlinearity and fractional induced resolution factor due to nonuniformity were examined. The results are shown in Fig. 21. Our conclusion is that the hadronic performance of the calorimeter degrades significantly for peak damages > 30%[6].

4. Use of a Shower-Max Detector to Reduce Sensitivity to Radiation Damage

We construct a model for the effects of radiation damage on an EM calorimeter and use that model to investigate how a shower-max detector might be used to monitor and partially compensate for that radiation damage as an extra use of the shower-max detector besides the main physics purpose. The idea is that particles which shower deep in the tower, producing a small signal in the shower-max detector, are less affected by the damage than those particles which shower early in the most severely damaged part of the tower. If the depth of the EM calorimeter is big enough, and there is no other damage, the total energy deposition in the EM calorimeter is independent of the energy deposited in the shower-max detector. If there is radiation damage, the total energy deposition will be correlated with the energy deposited in the shower-max, depending on where the shower starts.

If we adjust the gain to keep the mean energy deposit at a fixed value, then the width, and the "constant term" in the energy resolution will be increased. We used EGS to produce 150 and 250 GeV incident electrons into our model tower according to the SDC Technical Design Report for the endcap calorimeter. The results are shown in Fig. 22.1-22.2. One can see that, at the same radiation damage level, the data corrected by the shower-max detector have a smaller "constant" term, such that the energy resolution is roughly improved by a factor of 2 [25].

Summary

Several physics topics have been studied using SSCSIM. The goal has been to define and justify the choice of calorimeter parameters for the SDC. We have taken the results obtained by the Fermilab SDC software group and summarized the physics requirements for the SDC calorimeter in Table 7.

References

[1] W. Wu, *Study of Top Mass Measurement by using SSCSIM*, SSC-SDC-F-32, July 13, 1990.

[2] A. Para, A. Beretvas, K. Denisenko, N. Denisenko, D. Green, H. Iso, G. P. Yeh and W. Wu, *Jet Energy Resolution of the SDC Detector*, Fermilab-TM-1720 or SDC-90-00149, Dec. 6, 1990.

[3] F. Abe et al., *Jet-fragmentation Properties in $p\bar{p}$ Collisions at $\sqrt{s}$ = 1.8 TeV, Phy. Rev* **65**, 968 (1990).

[4] W. Wu, A. Beretvas, D. Green and J. Marraffino, *Hadronic and Electromagnetic Transverse Calorimeter Segmentation*, Fermilab-FN-589, April 1992.

[5] D. Green, A. Beretvas, K. Denisenko, N. Denisenko, J. Marraffino, A. Para and W.Wu, *Depth Requirements in SSC Calorimeters*, Fermilab-FN-570, August 1991.

[6] A. Beretvas, D. Green, J. Marraffino and W.Wu, *Hadronic Energy Resolution and Radiation Damage*, Fermilab-FN-582, March 1992.

[7] W. Wu, *Radiation Damage Impacts to the Jet Energy Resolution*, SSC-SDC-F-72, April 2, 1991.

[8] W. Wu, A. Beretvas, K Denisenko, D. Green, J. Marraffino and A. Para, *Monte Carlo Simulations of 'compensation' in a Calorimeter*, Fermilab-FN-579, January 1992.

[9] A. Beretvas, et al., *Beam Tests of Composite Calorimeter Configurations from Reconfigurable-Stack Calorimeter*, August 17, 1992. Accepted by N.I.M.

[10] W. Wu, A. Beretvas, D. Green and J. Marraffino, *Study of the Process H(800)* $\rightarrow Z_1\, Z_2, Z_1 \rightarrow q\bar{q}, Z_2 \rightarrow \tau_1\tau_2, \tau_{1,2} \rightarrow \rho\nu$ *for the SDC Calorimeter,* Fermilab-FN-598, Nov. 1992.

[11] J. Freeman et al., *The CDF Upgrade Calorimetry*, FNAL CONF/07, Proceedings of the 2nd International Conference on Calorimetry in High Energy Physics, Capri, Italy, Oct. 1991.

[12] *An Expression of Interest to Construct a Major SSC Detector*, GEM TN-91-1, SSC EO1-0020, July 8, 1991.

[13] W. Wu, *Investigation of the Problem of* $H \rightarrow 2$ *gammas*, SSC-SDC-F-114, May 28, 1992.

[14] W. Wu, *Investigation of the Problem of* $H \rightarrow 2$ *gammas* (II), SSC-SDC-F-115, June 28, 1992.

[15] W. Wu, *H0(80-125 GeV)* $\rightarrow 2$ *gamma Search and EM Calorimeter Resolution*, SSC-SDC-F-120, Dec. 15, 1992.

[16] C. Barter et al., *Detection of H0* $\rightarrow$ *gamma gamma at the SSC*, High Energy Physics in the 1990's, Snowmass, 1988.

[17] W. Wu, Argonne/Fermilab, *Results from Clustering Method from High Pt Z Jets*, SSC-SDC-F-60, Dec. 1990.

[18] W. Wu, Argonne/Fermilab, *Results from Clustering Method from Low Pt Z Jets*, SSC-SDC-F-63, Jan. 1991.

[19] W. Wu, *Installation of the Clustering Program into SHELL*, Fermilab SSC-SDC-F-111, May 1992.

[20] J. Marraffino, W. Wu, A. Beretvas, D. Green, K. Denisenko and A. Para, *"Massless Gaps" for Solenoid + Calorimeter*, Fermilab-TM-1766, November 1991.

[21] W. Wu, *Study on e/gamma Showers in SDC Calorimeter*, Fermilab SSC-SDC-F-92, Oct. 30, 1991.

[22] W. Wu, *The Thickness of the Front Material vs. the Energy Resolution*, Fermilab SSC-SDC-F-106, April 10, 1992.

[23] A. Beretvas, D. Green, J. Marraffino and W. Wu, *A Weighting Strategy for Compensating Leakage in the SDC Electromagnetic Calorimeter*, Fermilab-FN-587, April 1992.

[24] W. K. Sakamoto et al., *Nucl. Instr. and Meth.* **A294**, 179 (1990).

[25] A. Beretvas, D. Green, J. Marraffino and W. Wu, *Use of a Shower Maximum Detector to Reduce Radiation Damage Sensitivity in EM Calorimeter*, Fermilab-FN-600, Dec. 1992.

Appendix A

Structure of SSCSIM program

(EXTERNAL procedure names will not appear)

Meaning of Symbols:

```
.   ==> terminal node in the tree
*   ==> external procedure
>   ==> subtree node, expanded below
+   ==> multiply called terminal node
    ==> procedure calling externals
?   ==> module is in IF clause
(   ==> module is in DO-loop
```

****

```
SSCSIM
    |-----INIT
    |          |-----READCAR
    |          |(----STAT
    |-----PHINIT
    |(----NOISE                                  ( Reading a file )
    |(----EVENT    >                             ==================
    |(?---TAGLEPTO
    |          |(???-ETAPHI   >
    |((??-EVENT    >
    |((??-EVENT1   >
    |((?--SELECT
    |(((?+CALOR
    |          |-----TOCAL
    |          |??---BFIELD   +
    |          |?----ETAPHI   >
    |          |?----G2
    |          |?----G1
    |          |?----DEPOSM                      ( Making LEGO )
    |          |          |(?---PROFILE  >        ==============
    |          |          |(----CRACK    +
    |          |          |(----LEGOM
    |          |?----DEPOSH
    |          |          |(?---PROFILE  >
    |          |          |(----CRACK    +
    |          |          |(----LEGOH
    |          |?----DEPOS
    |                     |(?---PROFILE  >
    |                     |(----CRACK    +
    |                     |(----LEGO
    |(((--TRACK
    |(((--CJETFIND
    |          |((---CRECOVER +
    |(((--EVENT    >
    |(((--EVENT1   >
```

```
##########################################################################
     |
     |
     |                                                  ( Doing analysis )
     |                                                   ================
     |
     |                          #################
     |
     |((---PHANAL
     |          |((---TAGFIL    >                      ( Quark method )
     |          |((---XMASS     >                       ==============
     |          |                #################
     |          |((?--ANALEPTO
     |          |          |(----PARENT    +
     |          |          |((---BFIELD    +
     |          |          |((?--ETAPHI    >
     |          |          |((?--JETVECM   >            ( Lepton analysis )
     |          |          |((??-ETAPHI    >            ====================
     |          |          |((??-JETVECM   >
     |          |          |((??-BFIELD    +
     |          |          |((?--ETAPHI    >
     |          |          |((?--ETAPHI    >
     |          |          |-----BFIELD    +
     |          |          |-----ETAPHI    >
     |          |##################################
     |          |((---PARENT    +
     |          |(((?-MCORR     >
     |          |(((?-ETAPHI    >
     |          |((---PARENT    +
     |          |(((--MCORR     >
     |          |(((--ETAPHI    >
     |          |(((--PARENT    +                      ( Jet analysis )
     |          |(((--MCORR     >                       ==============
     |          |(((?-ETAPHI    >
     |          |(((?-PARENT    +
     |          |((---MCORR     >
     |          |(((--ETAPHI    >
     |          |(((--XMASS     >
     |          |(((--FRAGMENT
     |          |          |-----PARENT    +
     |          |(((--JETVEC    >
     |          |-----XMASS     >
     |          |-----XMASS     >
##########################################################
     |(----CPHANAL
     |          |-----TAGFIL    >
     |          |-----XMASS     >
     |          |((---CQUARK
     |          |          |-----PARENT    +
     |          |          |(----MCORR     >
     |          |          |(?---ETAPHI    >
     |          |          |(?---PARENT    +
     |          |          |-----MCORR     >
     |          |          |(----ETAPHI    >
     |          |          |(----PARENT    +
     |          |          |(----MCORR     >            ( Clustering method )
     |          |          |(?---ETAPHI    >            ====================
     |          |          |(?---PARENT    +
     |          |          |-----MCORR     >
     |          |          |(----ETAPHI    >
```

```
     |          |          |(----PARENT    +
     |          |          |(----MCORR     >
     |          |          |(?---ETAPHI    >
     |          |((---CRECOVER +
     |          |(((?-JETVEC    >
     |          |(((?-CINVESTI
     |          |          |-----XMASS     >
     |          |(((?-CHIGHPT
     |          |          |(----JETVEC    >
     |          |          |(----CRECOVER +
     |          |          |(----JETVEC    >
     |          |          |(----XMASS     >
     |          |(((?-CLOWPT
     |                     |-----CRECOVER +
     |                     |(?---JETVEC    >
     |                     |((---JETVEC    >
     |                     |((---XMASS     >
     |                     |((?--CLOWPTCK
     |                     |          |?----XMASS     >
     |
##########################################################################
     |
     |
     |                                          ( Produce results )
     |                                          ==================
     |(----PLOT
     |          |-----GETC
     |(----PHYSICS

##########################################################################
```

Sub-node flow-chart
==========

```
============
Node name ==> EVENT
============

 EVENT
     |?----GETFIL    +
     |?----GETHEP    >

========
name ==> ETAPHI
========

 ETAPHI

============
Node name ==> EVENT1
============

 EVENT1
     |?----GETFIL1
     |?----GETFIL    +
     |-----GETHEP    >
```

```
=============
Node name ==> PROFILE
=============

 PROFILE

=============
Node name ==> TAGFIL
=============

 TAGFIL
     |(?---TAG

=============
Node name ==> XMASS
=============

 XMASS

=============
Node name ==> JETVECM
=============

 JETVECM

=============
Node name ==> MCORR
=============

 MCORR

=============
Node name ==> JETVEC
=============

 JETVEC

=============
Node name ==> GETHEP
=============

 GETHEP
     |-----PARTYP
```

```
C THESE ARE  EXAMPLE DATA CARDS FOR RUNNING PROGRAM UPDATED SSCSIM
c
c     Weimin Wu, Oct 20, 1992
c
C
c    [ A ]    Events and the file
C
LIST          ! print the list of cards to be read
C             ! as a comment if starts with single C
NUEV  500
c             ! number of events to be processed
NOVE 15
c             ! number of events to overlay on a given event
c             ! Notice: if NOVE is not zero, you must use different
C             ! command to run the program
NTAG  1
c             ! number of partons to tag
TAGP  23
c             ! The parton's ID
c=====================================================================
c
c    [ B ]    Quark or clustering for Jets
C
TAGL "OFF"
c             ! Do you want to tag and analyze the lepton or
c             ! analyze jet?
c             ! Yes, Tag and analyze lepton. No, analyze jet.
c             ! If yes, you have to look at TAGLEPTON routine, to
C             ! see which lepton you want to analyze, and make
c             ! corresponding ID changes
CLUS "OFF"
c             ! Do you wish to use the clustering algorithm to find
c             ! jet?
HICL "OFF"
c             ! Do you want to find High Pt jet only?
LOCL "OFF"
c             ! Do you want to find low and high Pt jets ?
c
STRP "TRUE"
C             ! If you want to study shower-max "strips" ?
c
c=================================================================
c
c    [ C ]    Detector configuration and geometry
c
ETAL -1.5
c             ! minimum value of ETA,the pseudorapidity
DETA 0.10
c             ! the size of tower in pseudorapidity (HAD section)
PHIL 0.
c             ! mimimum value of PHI,the azimuthal angle
PHIM 6.283
c             ! maximum value of PHI,the azimuthal angle
DPHI 0.10
c             ! the size of tower in azimuthal angle (HAD section)
RADC 230.
c             ! geometry size for Solenoidal detector as  radius in CM
HALF 450.
c             ! geometry size for Solenoidal detector as  half of length
```

```
c            ! in CM
DEPT 10.
c            ! Total length of the calorimeter(EM+HAD) in unit of Lambda
XRAD 22.
c            ! EM section length in unit of radiation length (X0)
IEMF 1
c            !  Material for HAD section (EM section always uses Pb)
c            !   1    Pb,    2    Fe
FEHG 1.
c            ! 0 the EM section cell has same cell size with Had section
C            ! 1 ....................  half........................
BFIE 18.0
c            ! B field  in unit T
c=========================================================================
c
c    [ D ]  Calorimeter resolution and shower profile
c
HADR 0.5
c            ! constant we used for energy smearing of hadrons
c            !  (stochastic term)
HADC 0.03
c            ! constant we used for energy smearing of hadrons
c            !   (constant term)
EMSR 0.2
c            ! constant we used for energy smearing of electron
c            !   (stochastic term)
EMSC 0.01
c            ! constant we used for energy smearing of electrons
c            !   (constant term)
A1C0 0.7
c            ! constant we used for transverse hadron shower profile
c            !    parameters
A2C0 0.3
c            ! constant we used for transverse hadron shower profile
c            !    parameters
B1C0 2.0
c            ! constant we used for transverse hadron shower profile
c            !    parameters
B2C0 7.0
c            ! constant we used for transverse hadron shower profile
c            !    parameters
EMWI 1.
c            ! constant we used for transverse electron shower profile
c            !    parameter
DVEP 0.001   ! vertex smearing in PHI direction

DVER 0.25    ! vertex smearing in radians in cm

DVEZ 0.25    ! vertex smearing in Z direction in cm

c=====================================================================
c    [ E ]    Compensation
c
ETOM 0.85
c            ! an exponent number which we used in H/E compensation,
c            ! which is not sensitive to the results,and it is in range
c            ! between 0.85 and 0.90
EEEH 1.25
c            ! ratio of the calorimeter effciencies for detecting low
```

```
c            ! energy electronic and hadronic energy deposition.If it is
c            ! 1.0,it means it is an perfect compensated detector for
c            ! electronic and hadronic energy deposition.For CDF detector,
c            ! the number is around 0.65
ETEO 1.
c            ! scale factor near 1 Gev which we used for E/H compensation
c=====================================================================
c    [ F ]   Logical control flags
ZONL "OFF"
c            ! if it is true,only Z decay production are processed
WONL "OFF"
c            ! if it is true,only decay production Ws are processed
ONEW "OFF"
c            ! if it is true,only one W of decay production is processed
BEND "TRUE"
c            ! if it is true,charged particle are bent in the field
COMP "TRUE"
c            ! if it is true,it is non-linear response of hadron
c            ! calorimeter
SMEA "OFF"
c            ! if it is true, energy smearing is provided
TRPR "TRUE"
c            ! if it is true,transverse shower profiles are provided
MCCO "OFF"
c            ! Do you want to make particle momentum corrections due to
c            ! B field
ADDN "OFF"
c            ! Do you want to add noise randomly on each tower?
RADI "OFF"
c            ! Do you want to make corrections for radiation damage
CRAK "TRUE"
c=====================================================================
c    [ G ]   Data analyze cut condition
c
ASNO 0.2     ! Add random noise to each cell with sigma ASNO of Gaussian width
C            ! in GeV
TOWR 0.1
c            ! tower threshold in calorimeter towers
PECU 0.
c            ! Pt (GeV/c) cut threshold of the final lepton(e) to be
c            ! analysed
PBCU 0.
c            ! Pt (GeV/C) cut threshold of the mother of final lepton
c            ! (electron)
HMCT 0.04
C            ! Cut threshold to identify electron (EM/EH)
c=====================================================================
c    [ H ]   Histogram and radious requirements
c
NRAD  1
c            !NUMBER OF DIFFERENT RADIUS POINTS
STEP  0.1
c            !STEP TO CALCULATE RADIS OF CIRCLE
RMIN  0.5
c            !MINIMUM VALUE OF RADIUS - FIRST POINT
LOUT  6
c            !output lun
MASS  10000.
c            ! Z0 MASS for histogram scale
END
```

Appendix C

```
$ SET DEF SSCPHY_USR:[wu.test]
$!
$!   Define file with data cards
$!
$ DEFINE/user FOR004 jettest_BIGPB_MIN0.cards
$!
$!   Run it
$!
$ RUN/NODEB SSCHEP_updated
fnpw05$dub1:[sscscr2]zp_10tev.HEP
jettest_BIGPB_MIN0.FILE
$!
$!   Done !
```

```
$ SET DEF SSCPHY_USR:[wu.test]
$!
$!   Define file with data cards
$!
$ DEFINE/user FOR004 jettest_BIGPB_MIN15.cards
$!
$!   Run it
$!
$ RUN/NODEB SSCHEP_updated
fnpw05$dub1:[sscscr2]zp_10tev.HEP
FNPW03$DUB0:[SSCSCR]MINBIAS_SDC.HEP
fnpw05$dub1:[sscscr2]zp_10tev.HEP
jettest_BIGPB_MIN15.FILE
$!
$!   Done !
```

Table 1

Top mass resolution variation with the granularity and the cone size

$\Delta\eta = \Delta\phi$		0.03	0.05	0.07	0.09
R = 0.3	dM/M (%)	9.96	11.28	14.91	17.37
R = 0.5	dM/M (%)	8.42	10.71	13.52	16.48
R = 0.7	dM/M (%)	11.78	12.83	14.01	19.53

Table 2

Top mass resolution variation with different detector effects at fixed granularity of 0.05 and cone size at 0.5

	No detector effect at all	Smearing	B Field	Profile	e/h	all together
dM/M (%)	10.7	10.9	10.9	10.9	11.5	12.2

Table 3

Radiation damage degrades the jet energy resolution

		E(mea.)/E(ori.)		(E(mea.)-E(ori.))/E(ori.)	
		Mean	Width	Mean	Width
Z_55					
	dD=0.1	0.987	0.009	0.012	0.009
	dD=0.3	0.963	0.025	0.036	0.029
	dD=0.5	0.942	0.041	0.057	0.044
zp_550					
	dD=0.1	0.986	0.008	0.013	0.008
	dD=0.3	0.963	0.021	0.037	0.024
	dD=0.5	0.940	0.046	0.062	0.039
zp_10 TeV					
	dD=0.1	0.984	0.008	0.014	0.006
	dD=0.3	0.960	0.020	0.040	0.021
	dD=0.5	0.936	0.036	0.066	0.032

Table 4

Di-jet mass resolution and jet energy resolution			
Case	m(Rec)/m(Gen)	sigma(m)/M	sigma(E)/E
Z'			
ideal (lead)	0.968	0.022	0.010
smearing (lead)	0.967	0.025	0.019
ideal (iron)	0.915	0.025	0.019
smearing (iron)	0.913	0.030	0.028
smearing (iron) e/h-corrected	0.966	0.028	0.022

Table 5

Overview of the Zt Mass Resolution

Resolution of Zt mass	Cases			
%	ETA Limit	Options	Exception	Cell Size
22.92	3	On		SM
21.41	3	On		EM
20.85	3	On	Noise/threshold	EM
19.63	5	On	Add 15 minbias	SM
19.52	3	On	Noise/threshold	SM
18.40	5	On	4 cm cracks	EM
17.36	3	Off		EM
17.02	3	Off		SM
16.80	5	On	2 cm cracks	EM
16.45	5	Off	4 cm cracks	EM
16.33	5	Off	4 cm cracks	SM
16.01	5	On		SM
14.48	5	Off	2 cm cracks	EM
14.22	5	On		EM
13.94	5	On	Noise/threshold	EM
13.93	5	On	Noise/threshold	SM
13.14	5	Off	2 cm cracks	SM
11.87	5	Off		EM
11.67	5	Off	15 minbias	SM
10.87	5	Off		SM

Table 6

Summary Results for Higgs (80-125 GeV) decay into 2 gammas
with background subtracted

Higgs Mass		80 GeV	125 GeV
	Width (GeV)	1.493	3.098
Super-resolution	Mean (GeV)	74.09	114.4
	Width/Mean	2.02%	2.71%
	Width (GeV)	3.218	6.031
Conventional Resolution	Mean (GeV)	74.03	116.3
	Width/Mean	4.35%	5.19%
Ratio of Higgs mass resolution of conventional/super		2.15	1.92

Table 7

Physics Requirements for SDC Calorimeter Parameters

Parameters	Process	Allowed Range
Hermiticity	H(800) $\rightarrow$ Z Z | | $\rightarrow \tau\,\bar{\tau}$ | | $\rightarrow \rho\ \nu$ | | $\rightarrow \pi\ \pi^0$ | $\rightarrow 2\ \gamma$	2 cm --- 4 cm (cracks radially at surface between modules, corresponds 4.4-8.8% energy loss in cracks, or holes < 0.9 - 1.7%)
Upstream (coil) Material	EGS with electron of 12.5-100 GeV incident at 90/30 degree to the EM stack which is similar to SDC Configuration	< 1.0 - 1.2 X_0
Angular Coverage	H(800) $\rightarrow$ Z Z | | $\rightarrow \tau\,\bar{\tau}$ | | $\rightarrow \rho\ \nu$ | | $\rightarrow \pi\ \pi^0$ | $\rightarrow 2\ \gamma$	$\lvert\eta\rvert > 5$
Total Depth	PP $\rightarrow$ Dijet at mass of 10 TeV (weight strategy)	D > 9 - 10 λ
EM Depth	EGS with electron of 12.5-100 GeV incident at 90/30 degree to the EM stack which is similar to SDC configuration	22 - 25 X_0 at sampling 0.5 X_0
HAD Material	EGS with electron of 12.5-100 GeV incident at 90/30 degree to the EM stack which is similar to SDC configuration	Fe is as good as Pb
Longitudinal Segmentation HAD	PP $\rightarrow$ Dijet at mass of 10 TeV	Rear section of 3 - 4 λ
EM Resolution HAD Resolution	PP $\rightarrow$ Dijet at mass of 100 GeV, 1000 GeV and 10 Tev at low and high Pt	$\frac{0.2}{\sqrt{E}} \oplus 0.01$ or better $\frac{0.5}{\sqrt{E}} \oplus 0.03$ or better
Speed	PP $\rightarrow$ Dijet at mass of 100 GeV, 1000 GeV and 10 TeV at low and high Pt	< 1 bunch crossing

Table 7 (con't)

Trigger	PP → Dijet at mass of 100 GeV, 1000 GeV and 10 TeV at low and high Pt Top → W & b | → c e ν	| Pt(e) | > 20 GeV
Compensation	PP → Dijet at mass of 100 GeV, 1000 GeV and 10 TeV at low and high Pt PP → Top pair at high Pt	| e/h -1 | < 0.3
Transverse HAD Segmentation	PP → Dijet at mass of 100 GeV, 1000 GeV and 10 TeV at low and high Pt	$\Delta\eta = \Delta\phi < 0.1$
Transverse EM Segmentation	Top → W & b | → c e ν (non-isolated e)	$\Delta\eta = \Delta\phi < 0.05$
Shower-max	H(800) → Z Z | | → $\tau\,\bar{\tau}$ | | → $\rho\ \nu$ | | → $\pi\ \pi^0$ | → 2 γ Top → W & b | → c e ν (non-isolated e)	Width < (0.05/8) cm Length < 0.2
Radiation Damage	LEB E data & BEPC data with EGS studies	Survive 10 years of SSC design luminosity at η around 2.5 for standard tile/fiber
Noise & Threshold	H(800) → Z Z | | → $\tau\,\bar{\tau}$ | | → $\rho\ \nu$ | | → $\pi\ \pi^0$ | → 2 γ	Noise < 100 MeV Threshold < 200 MeV
Vertex	Higgs (125 GeV) → 2 γ	0.001 in φ 0.25 cm in radians and z directions
Pileup	PP → Dijet at mass of 100 GeV, 1000 GeV and 10 TeV at low and high Pt Top → W & b | → c e ν H (800) → Z Z | | → $\tau\,\bar{\tau}$ | | → $\rho\ \nu$ | | → $\pi\ \pi^0$ | → 2 γ	10 times of SSC design luminosity still ok for above parameters

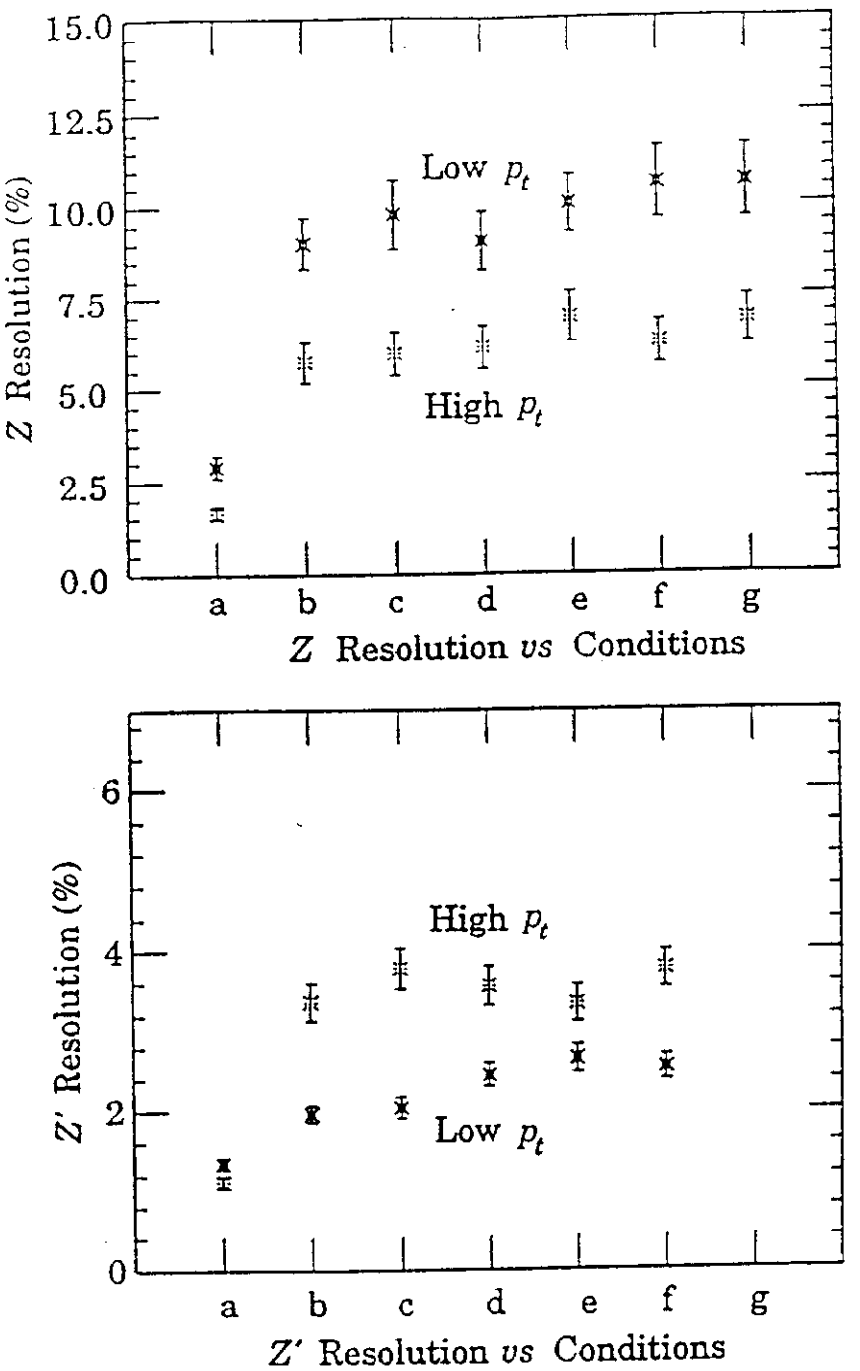

The fractional mass resolution for Z and 1 TeV Z' decays into dijets.

a. Perfect detector, no underlying event, finite cone R = 0.7.

b. Perfect detector, underlying events

c. As in b but with $0.15/\sqrt{E} \oplus 0.01$ for EM and $0.3/\sqrt{E} \oplus 0.02$ for HAD

d. As in c but with $0.5/\sqrt{E} \oplus 0.03$ for HAD

e. As in c but with $0.7/\sqrt{E} \oplus 0.04$ for HAD

f. As in d but with $0.25/\sqrt{E} \oplus 0.02$ for EM

g. As in d but with e/h = 1.3 for HAD

Fig.1

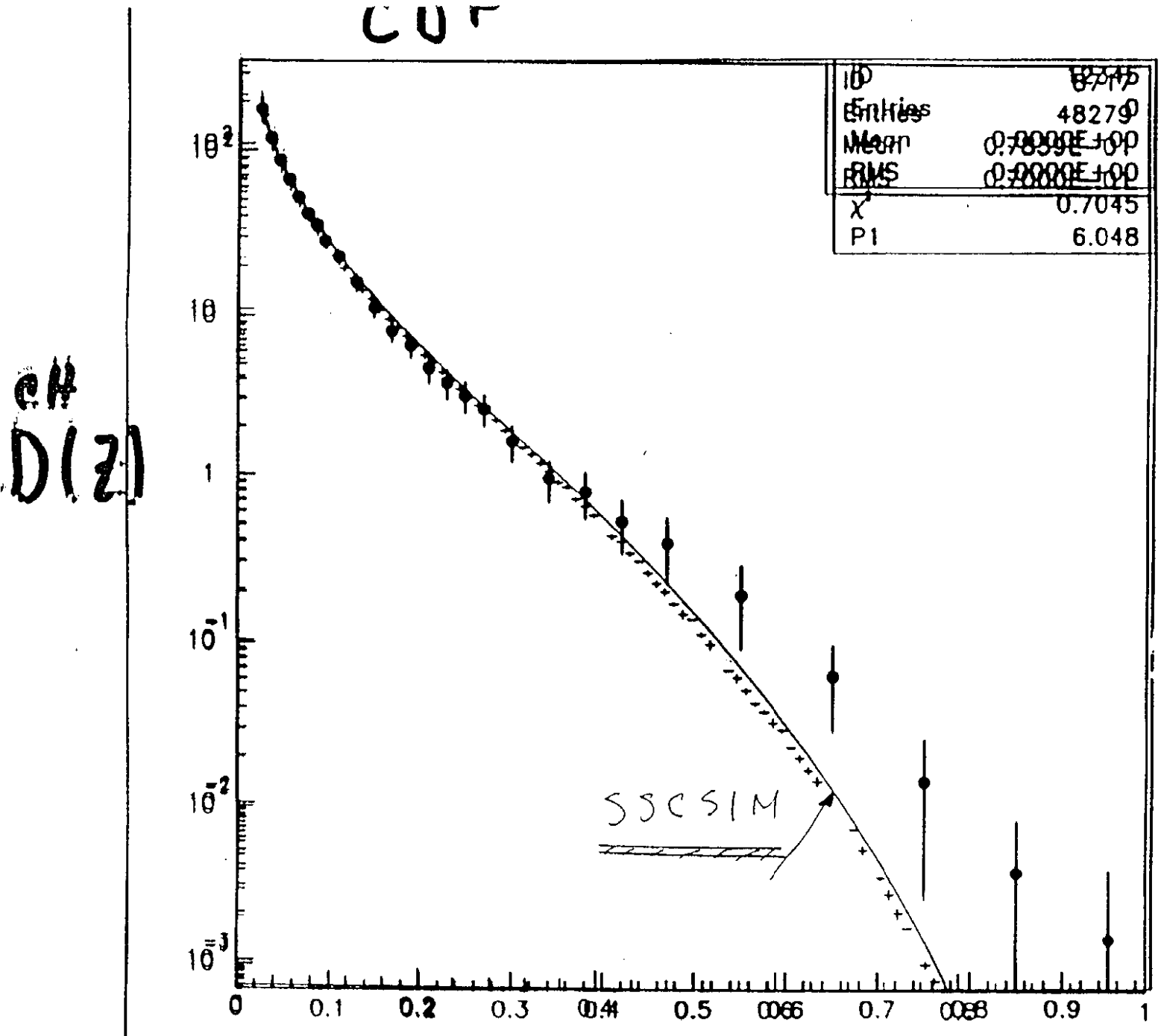

Fig.2 ISAJET and CDF frangmentation function D(z)

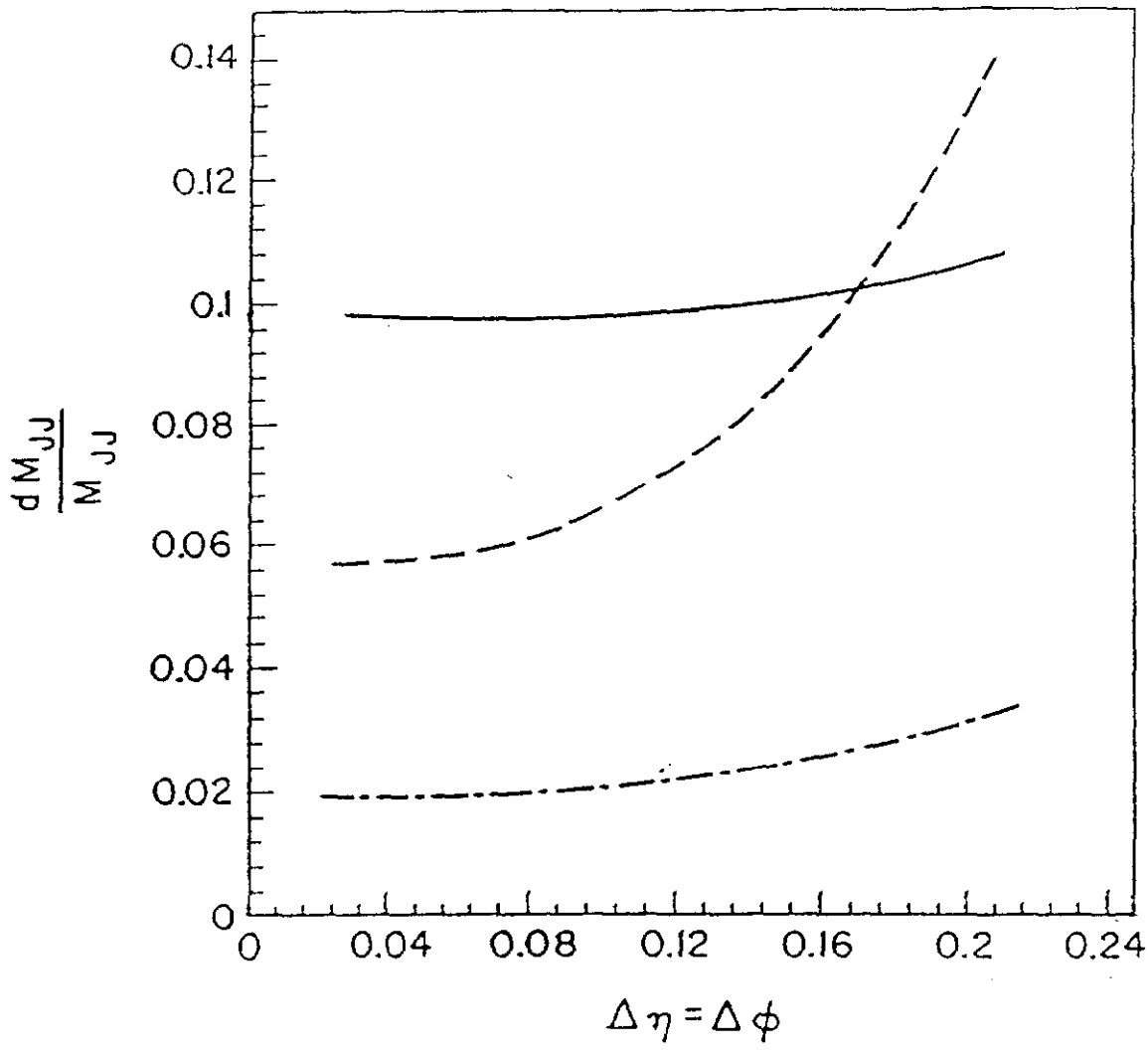

Fig.3 Dijet mass resolution as a function of the transverse segmentation of the calorimeter cells. The curves are Z with Pt = 55 GeV, solid, Z with Pt = 550 GeV, dashed, and a 10 TeV Z' produced at low Pt, dot-dashed.

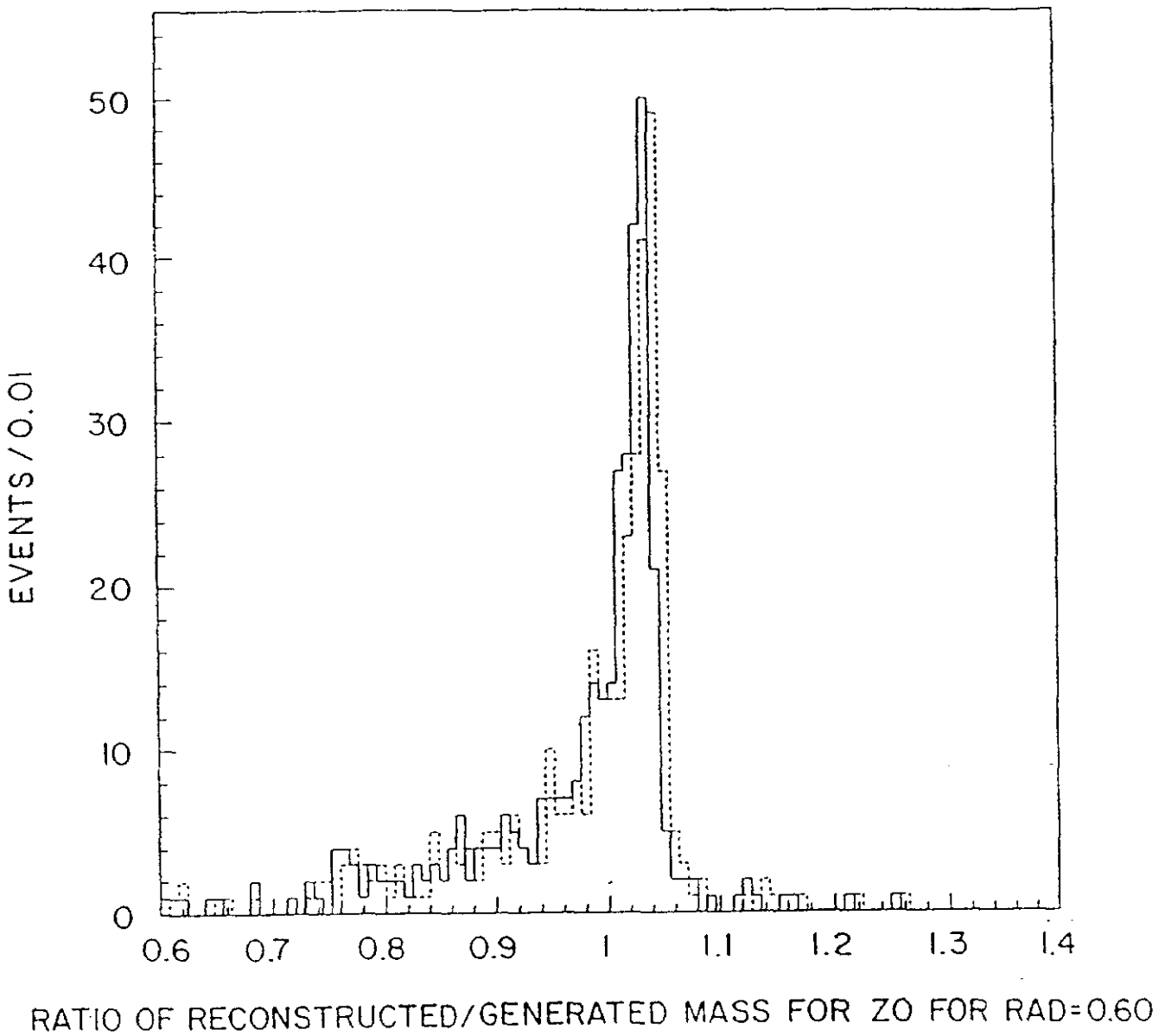

Fig.4 Histogram of the ratio of reconstructed to generated Z mass with a cluster cone size of R = 0.6. The EM section has towers of size $(0.05)^2$ while the HAD towers are $(0.05)^2$, solid, and $(0.1)^2$, dashed.

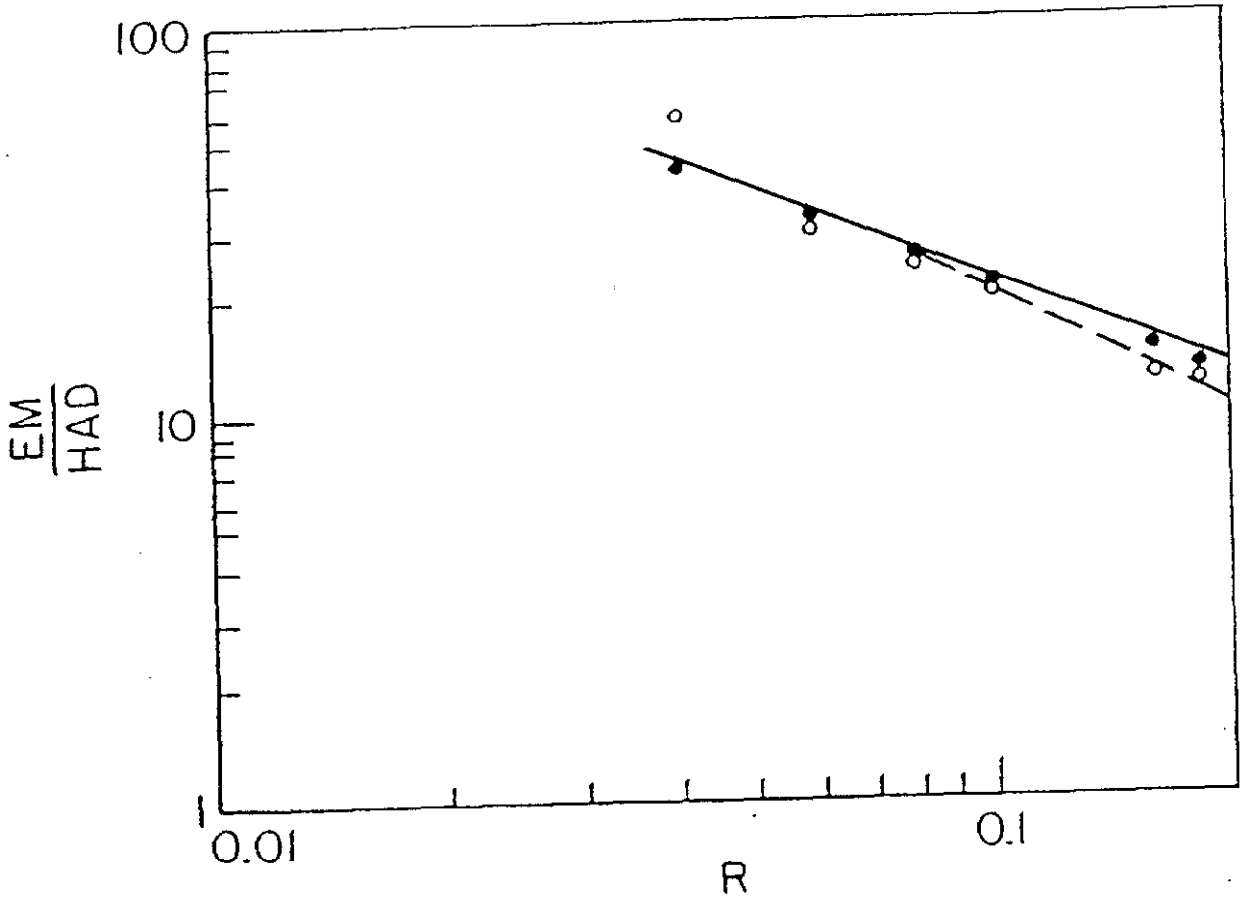

Fig.5 Plot of the ratio of energy in the EM to the HAD compartment of the calorimetry. The curves refer to EM segmentation of $(0.05)^2$ and HAD segmentation of $(0.05)^2$, solid, and $(0.1)^2$, dashed. The radius R refers to a cone centered on the cell where the maximum e energy is deposited.

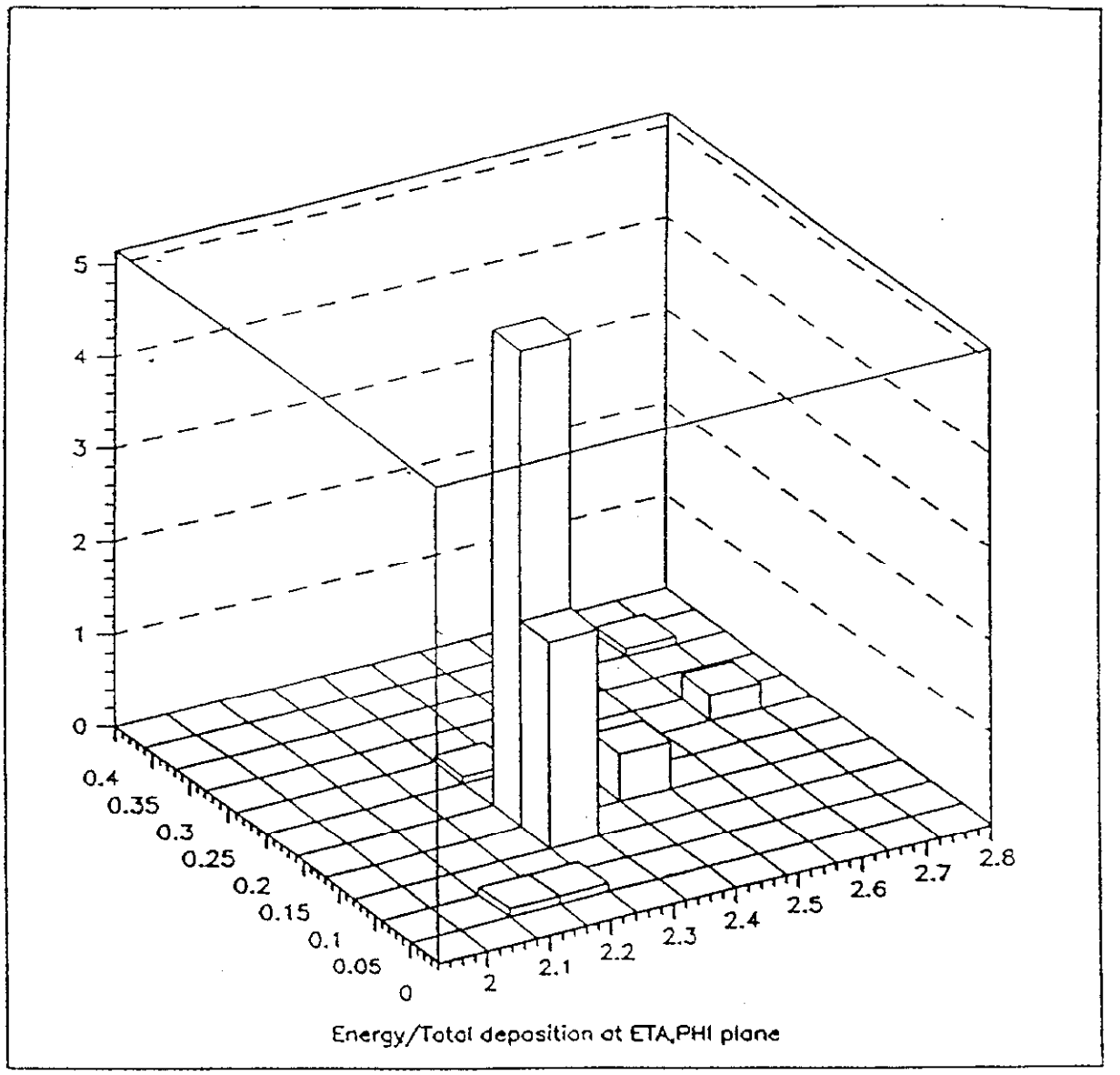

Fig.6 LEGO plot of the EM+HAD energy deposited near the e cell. The cell size is taken as $(0.05)^2$.

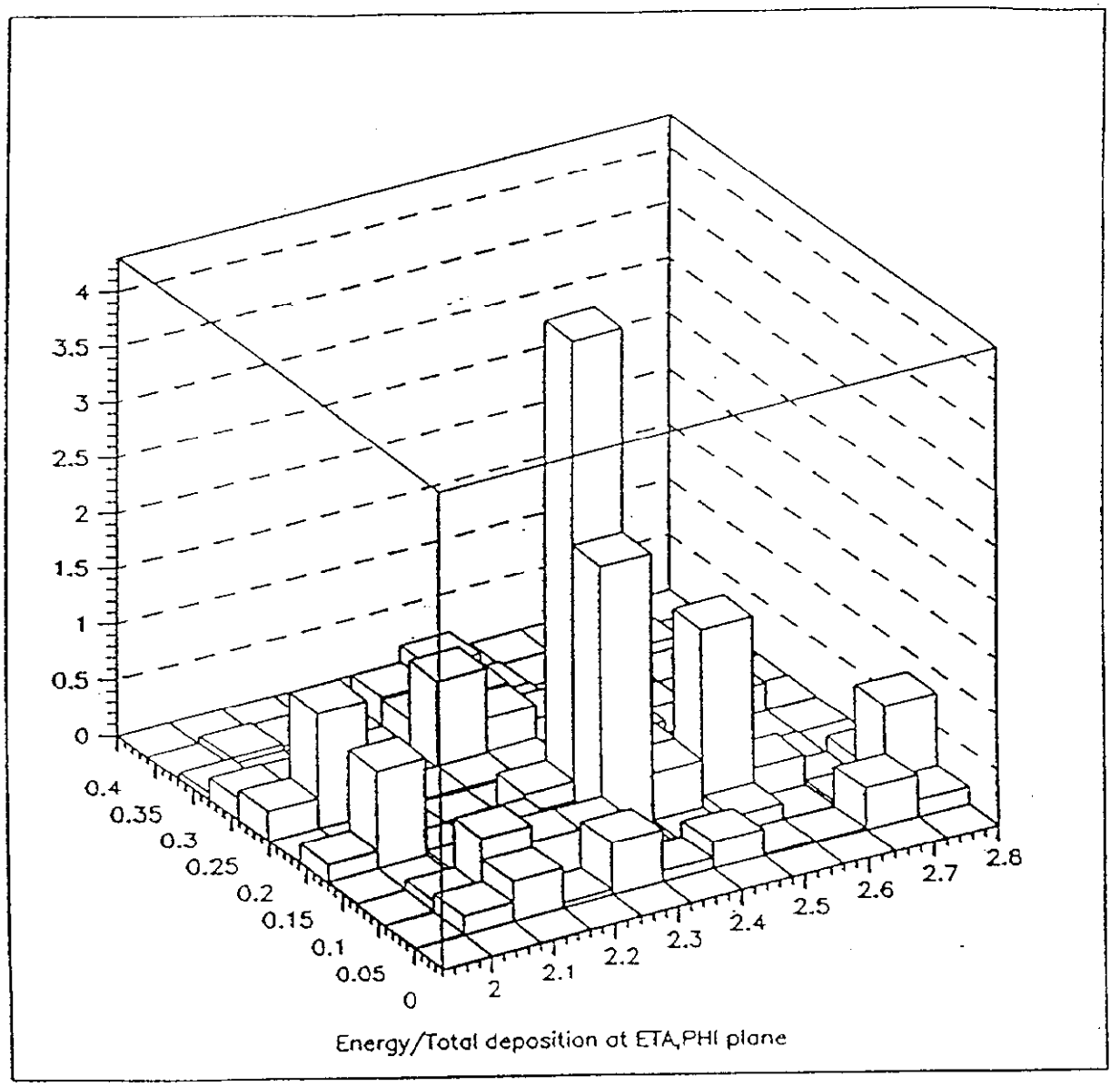

Fig. 7 LEGO plot as Fig.6 except the field is turned off. Note, in comparison to Fig.6, the sweeping effect of the field in removing nearby c frangments.

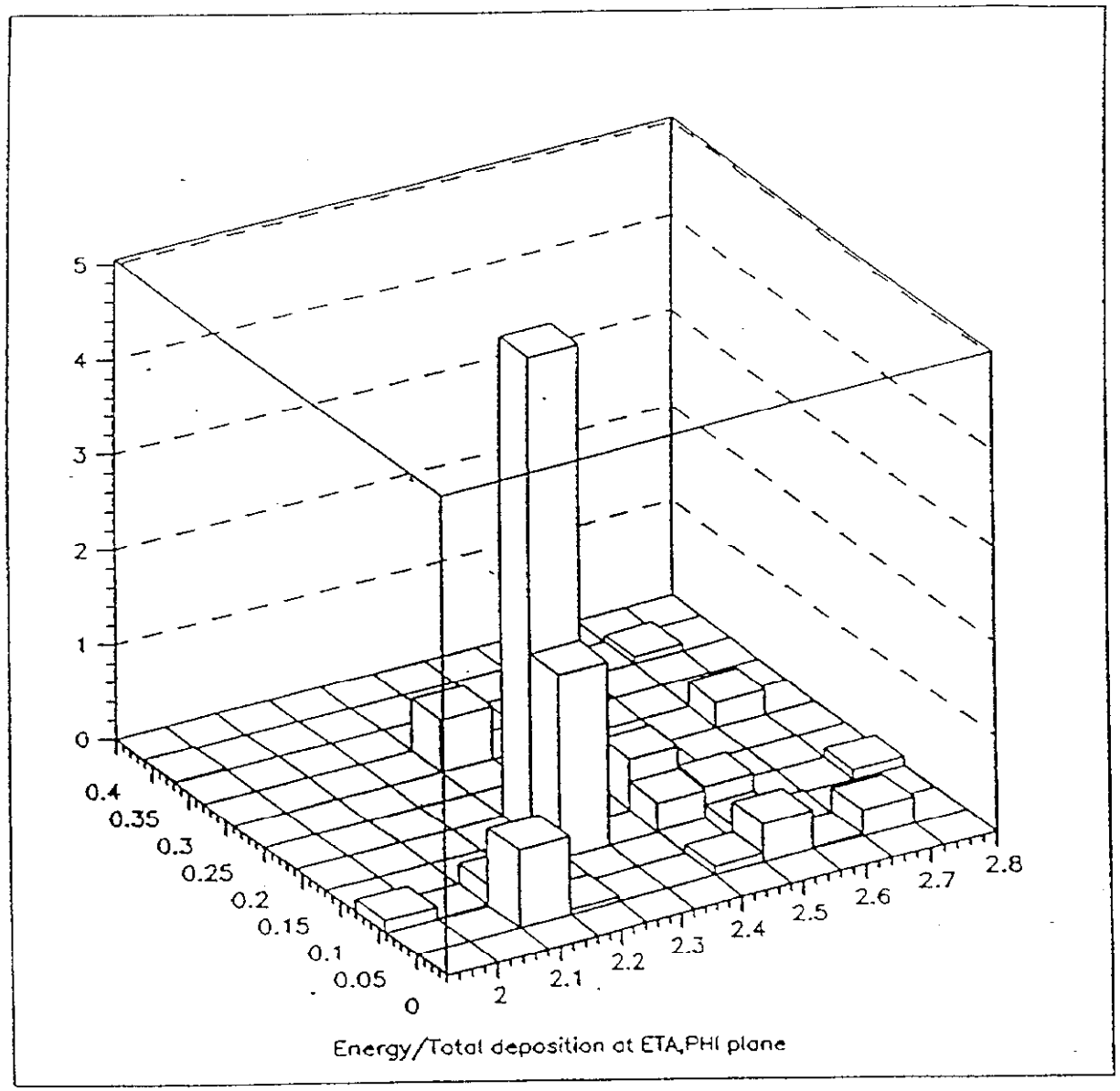

Fig.8 LEGO plot as in Fig.6 except that "minibias" events have been overlapped with the tt(bar) event. A Poisson distribution with mean of 15 has been assumed for high luminosity operation

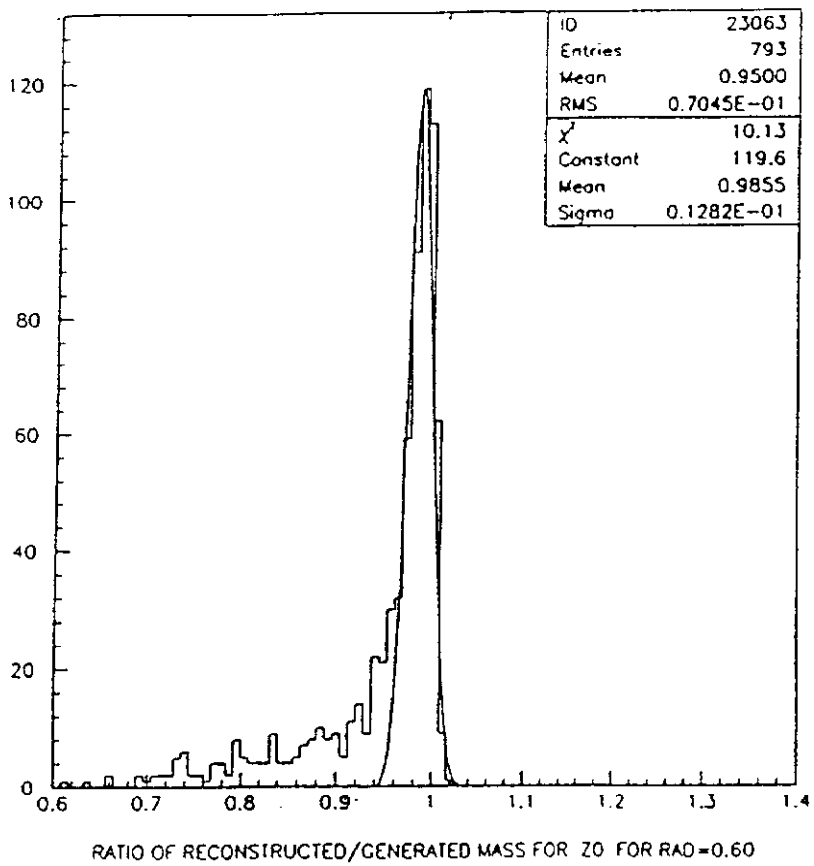

Fig.9 Histogram of the ratio of reconstructed to generated mass for 10 TeV dijets using a cone of radius R = 0.6. Only jet fragments are used in the calculation.

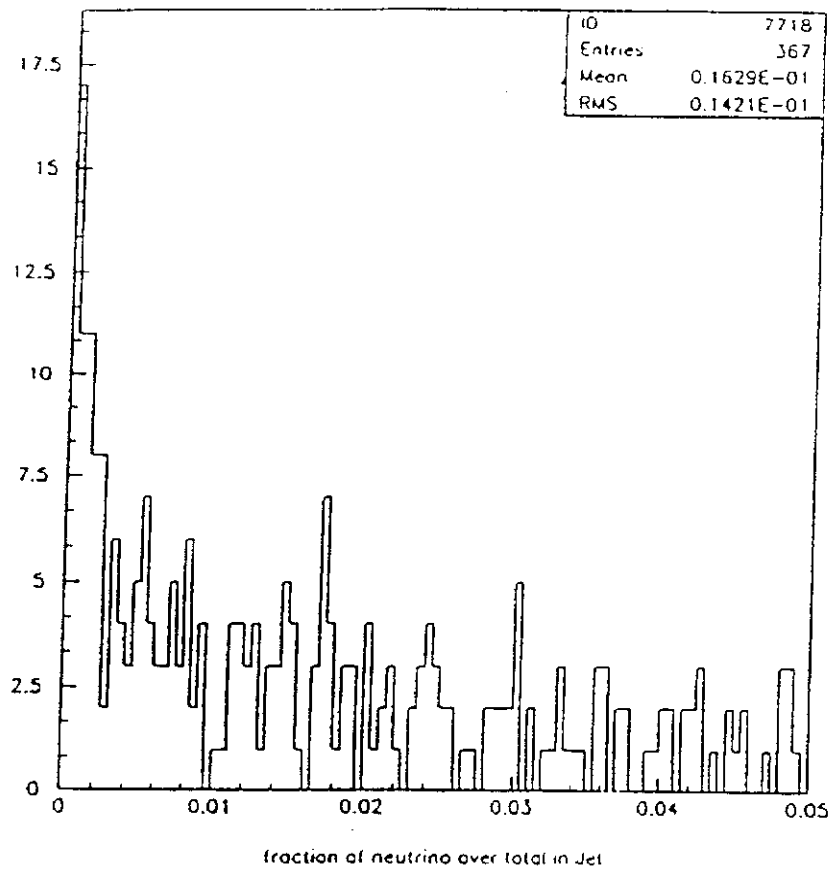

Fig.10 Histogram of the fraction of the jet energy carried away by neutrinos. For leading fragmentation this fraction would be equal to about 1/6

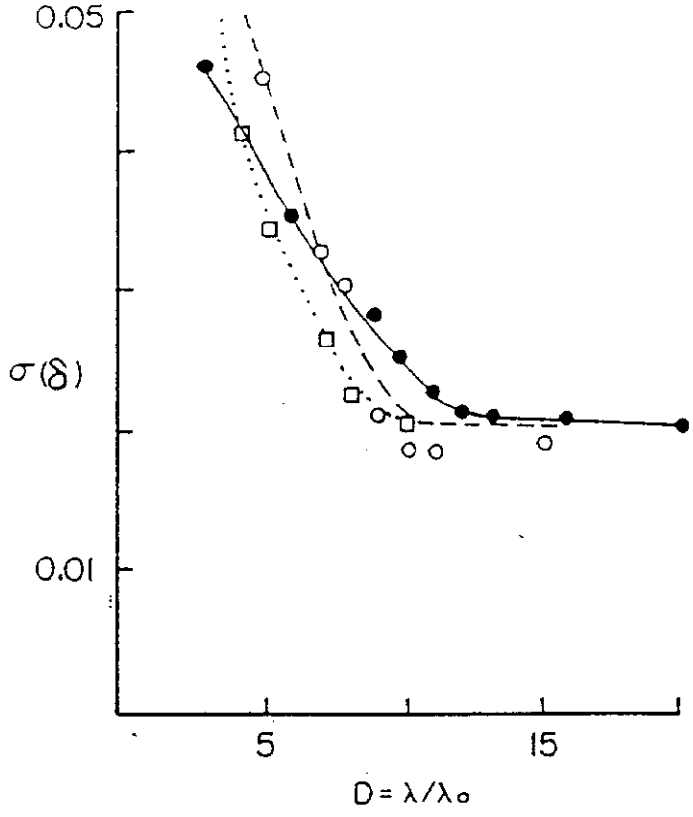

Fig.11 Error on the ratio of reconstructed to generated dijet mass as a function of the depth of the calorimetry for 10 TeV dijets; CITF •, WA1 o, Lab E, □, parametrizations.

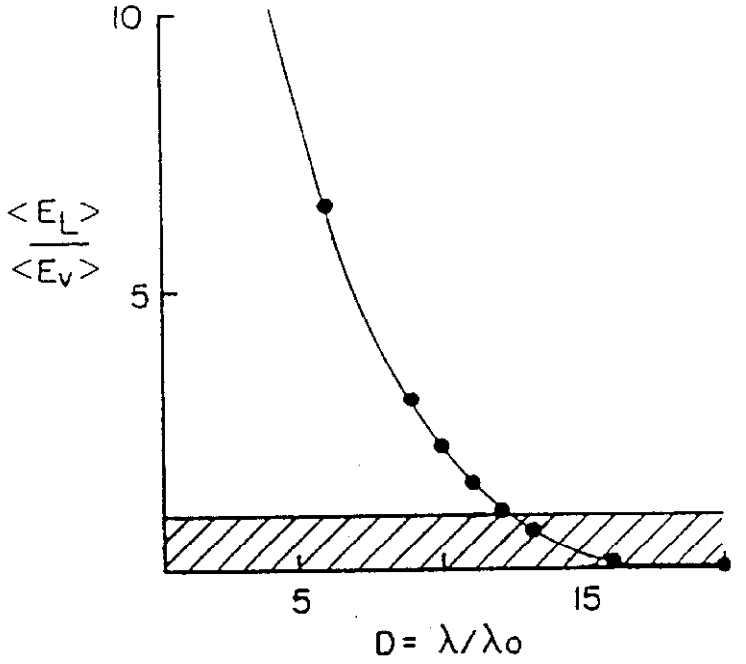

Fig.12 Ratio of mean leakage energy to mean neutrino energy as a function of the calorimeter depth. The hatched region corresponds to "leakage" dominated by neutrinos.

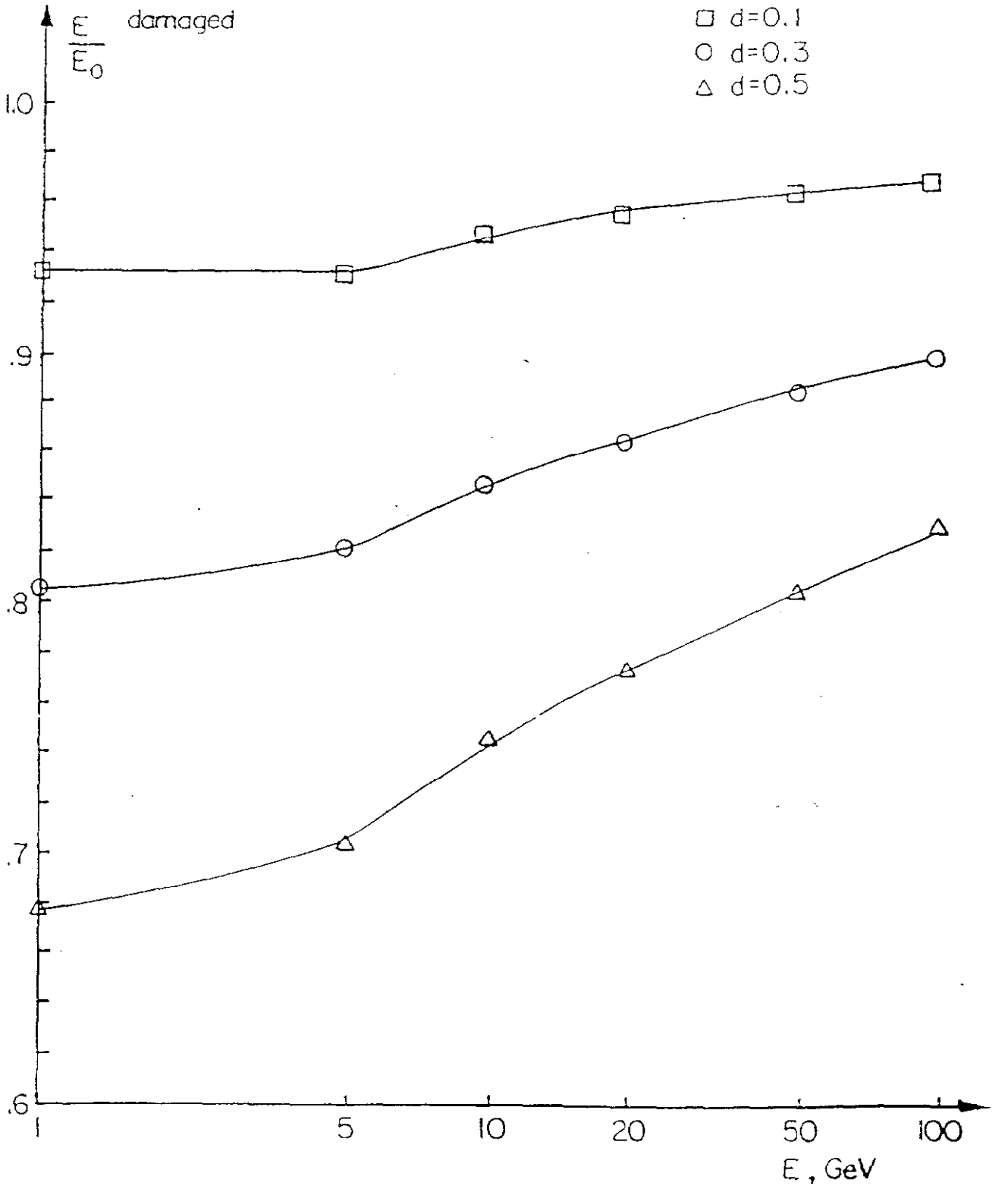

Fig.13 Mean fractional energy output as a function of incident e energy for maximum light loss d of 10, 30 and 50 %.

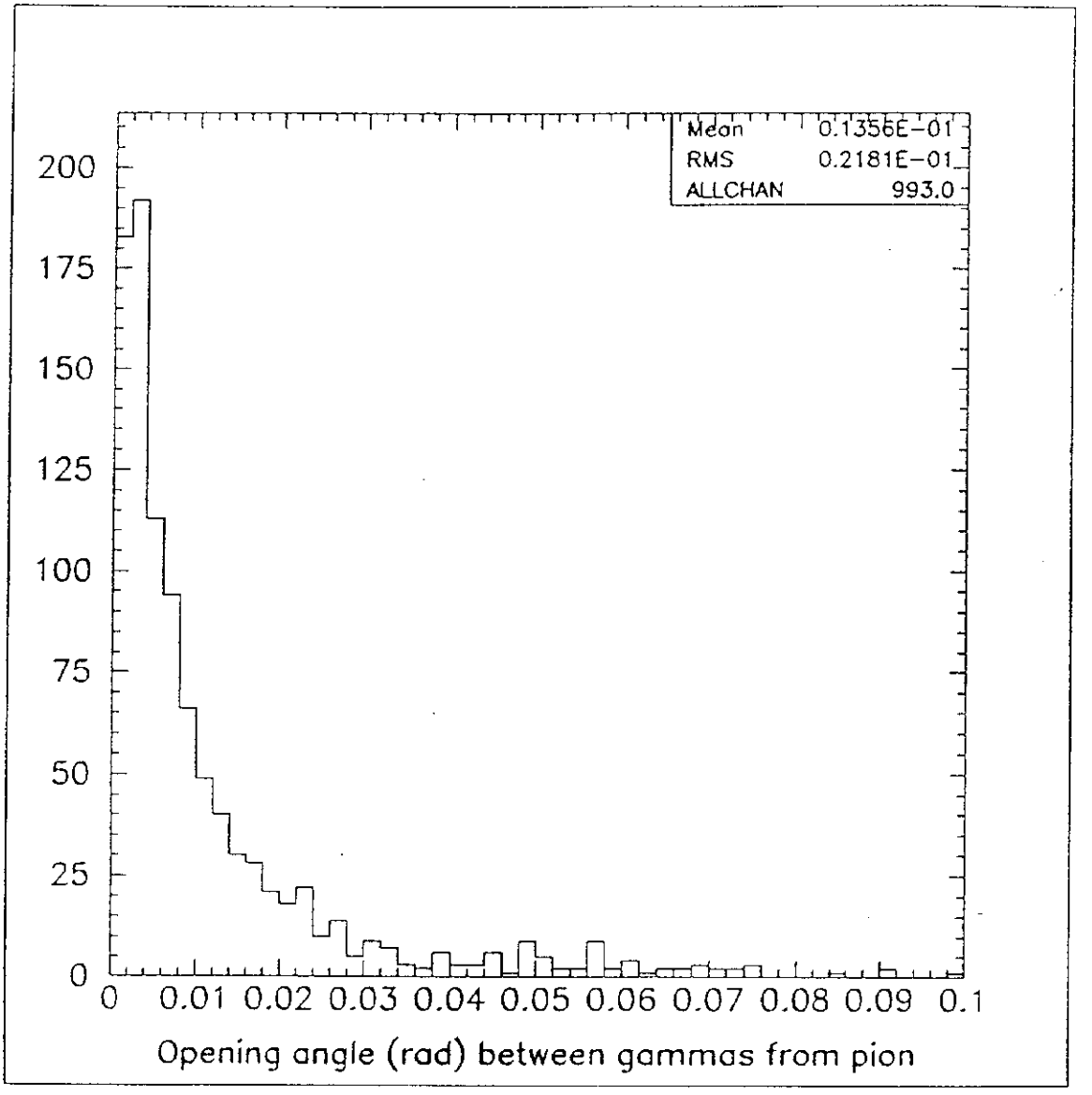

Fig.14 The opening angle between the two γ's.

in Z--> Tau+ Tau-, Tau(+/-)-->Rho(+/-) Nu, Rho(+/-)--> Pi0 Pi(+/-) and Pi0 -->Gamma Gamma decays

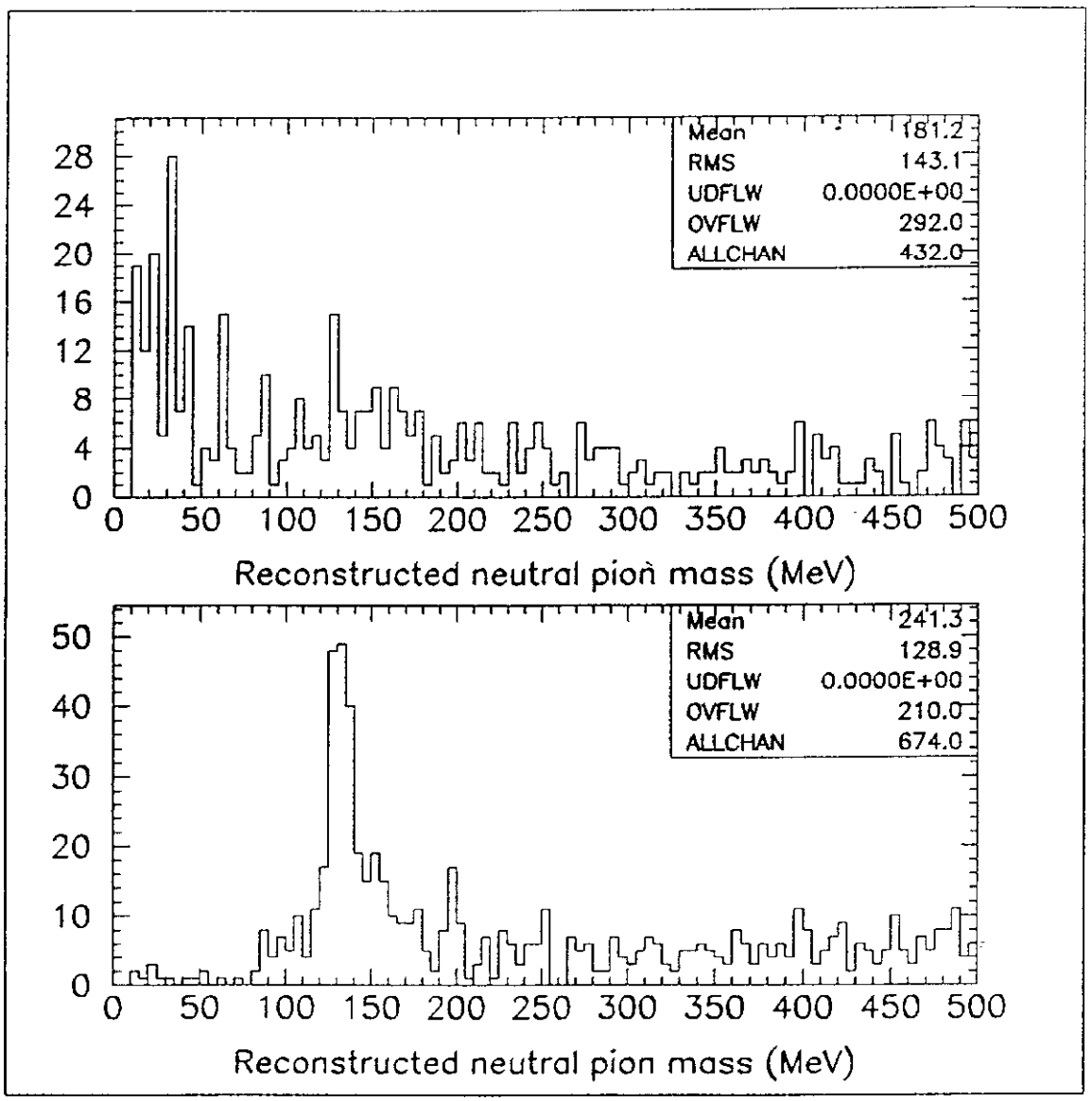

Fig.15.1-15.2 The mass of the reconstructed π^0 (GeV/c^2) (a) for EM calorimeter cell size of $\Delta\eta = \Delta\phi = 0.05$ (b) cell size $\Delta\eta = \Delta\phi = 0.00625$.

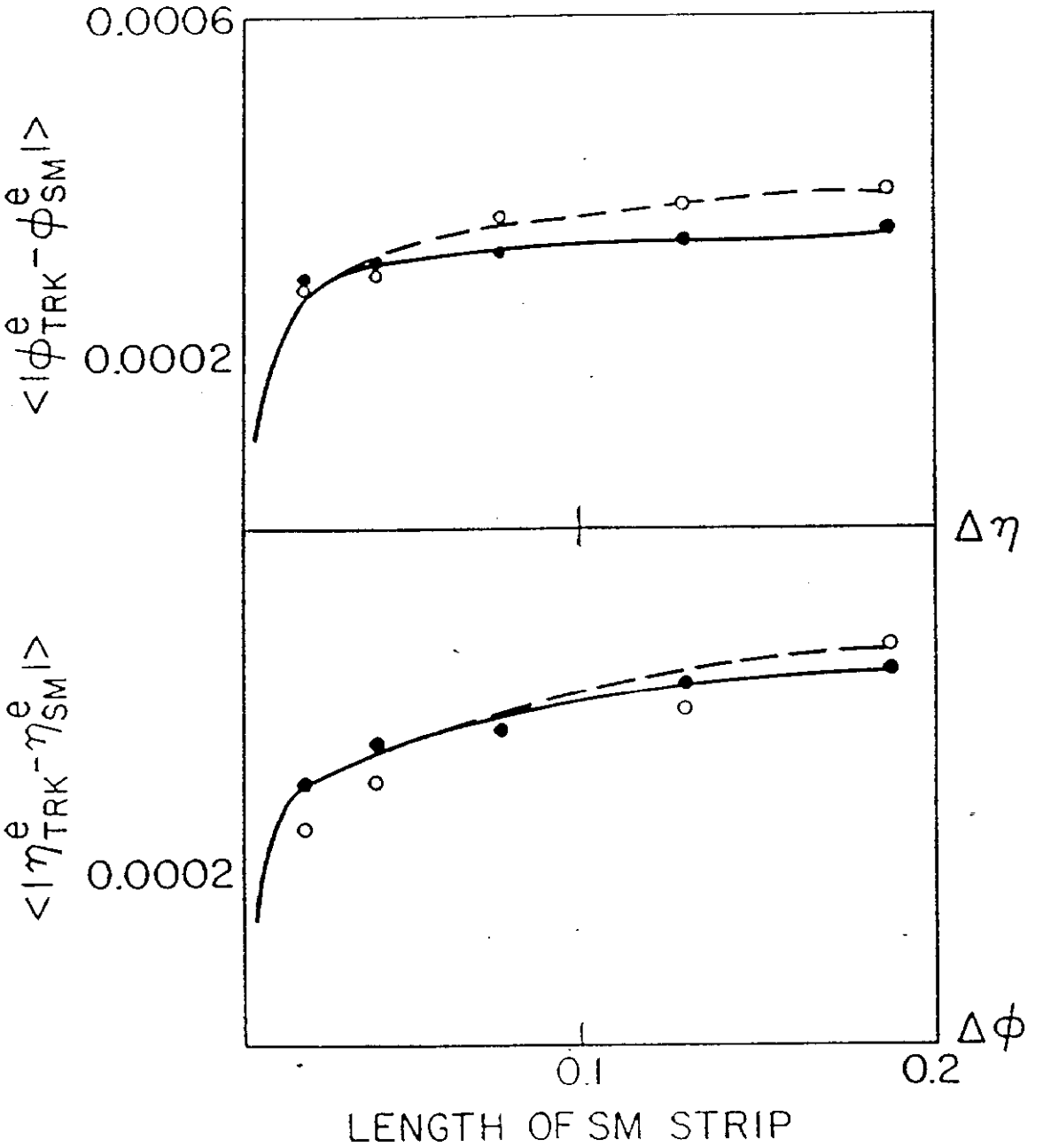

Fig.16 Plot of the mean deviation of the e track from the energy center of gravity as determined by a Shower Maximum (SM) detector as a function of the strip length. Strips are 0.05/8 wide in η or ϕ (crossed strips). The solid curve refers to $t\bar{t}$ events only. The dashed curve refers to the case where $t\bar{t}$ events have 15 minbias events overlapped.

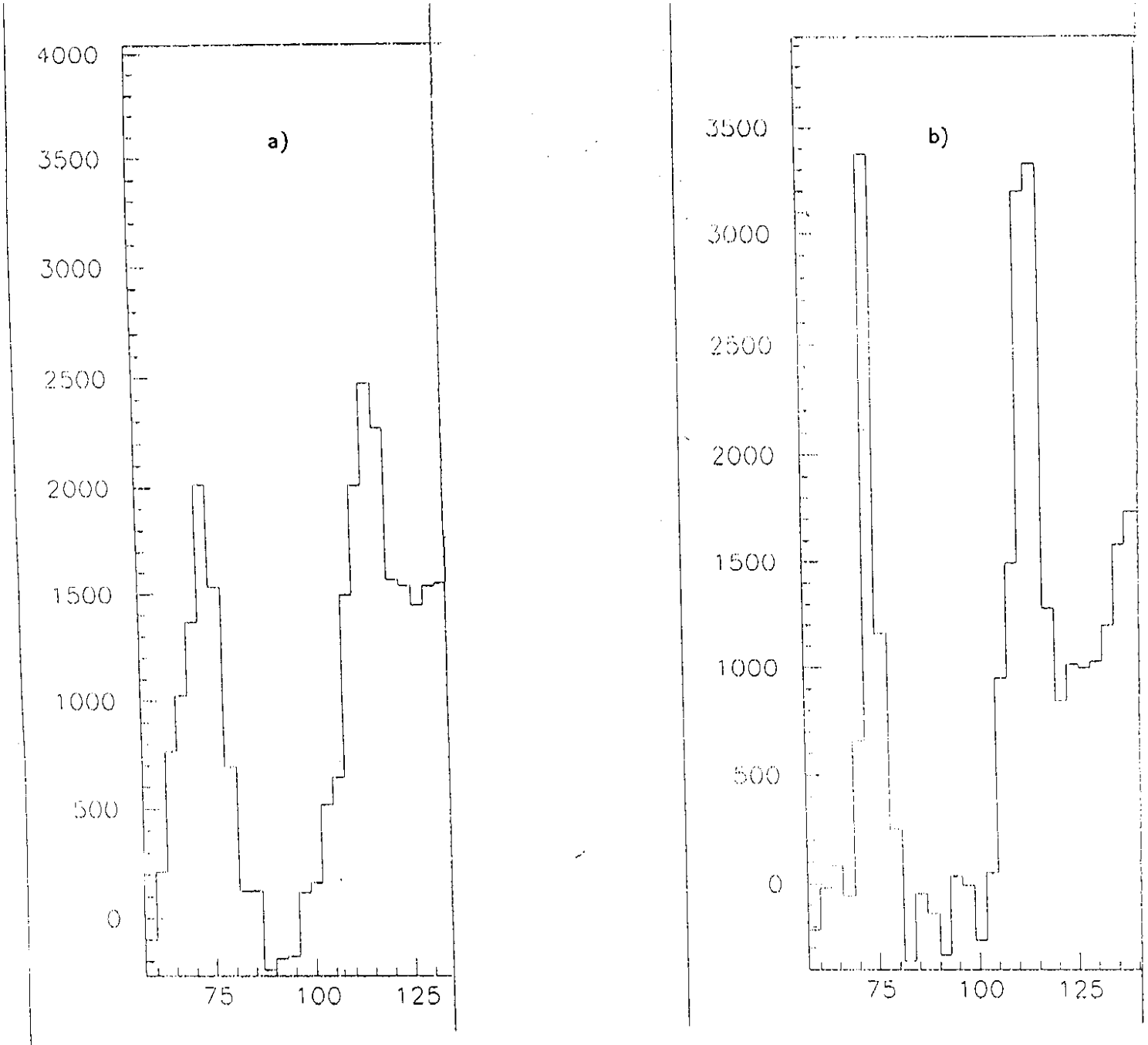

Fig.17 H--> Gamma gamma event with background subtracted for 80 and 125 GeV Higgs bosons.
a) SDC resolution
b) "super" EM calorimeter

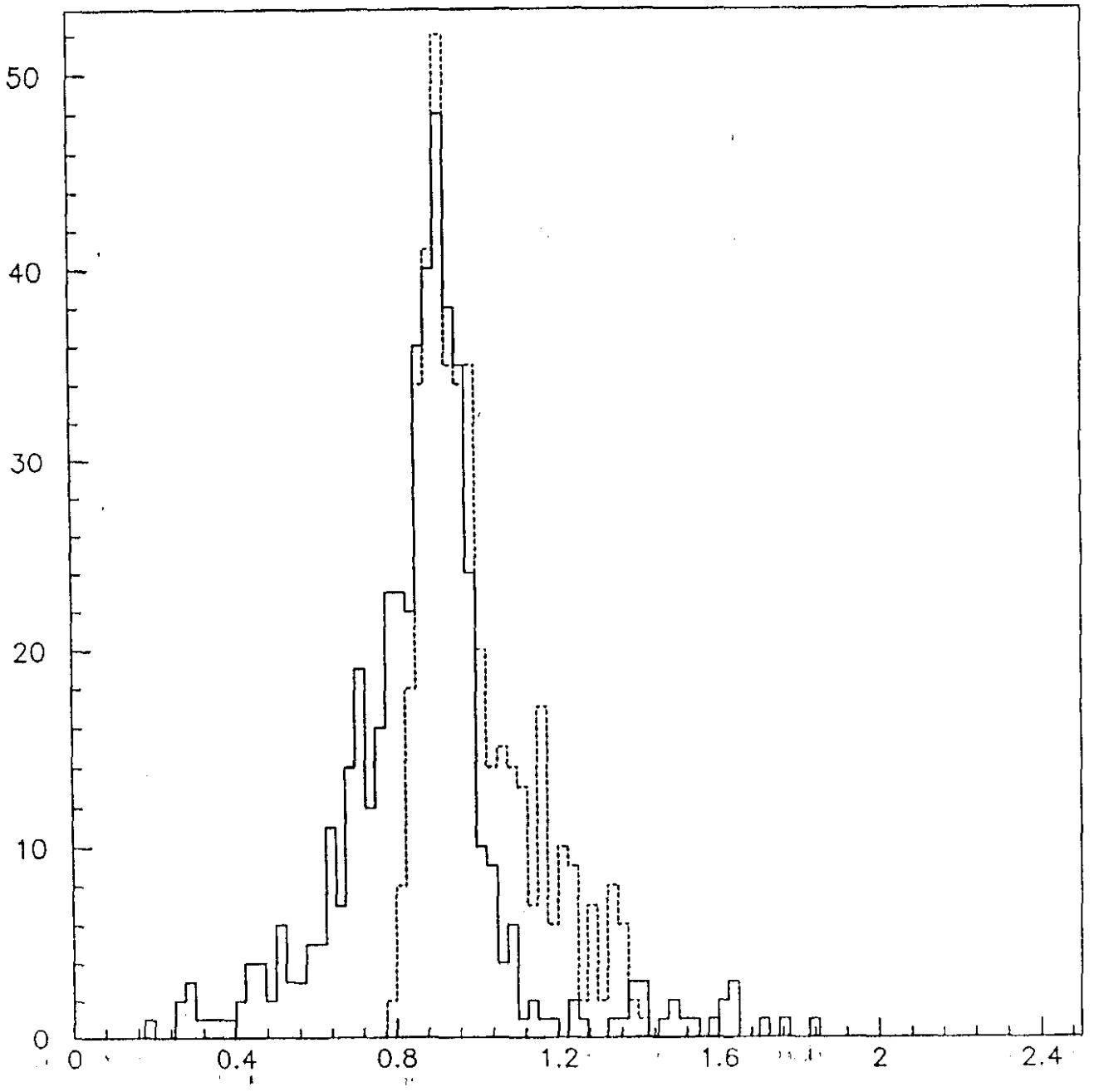

Fig.18.1 Z_55 RATIO OF RECONSTRUCTED/GENERATED MASS FOR ZO FOR RAD=0.70

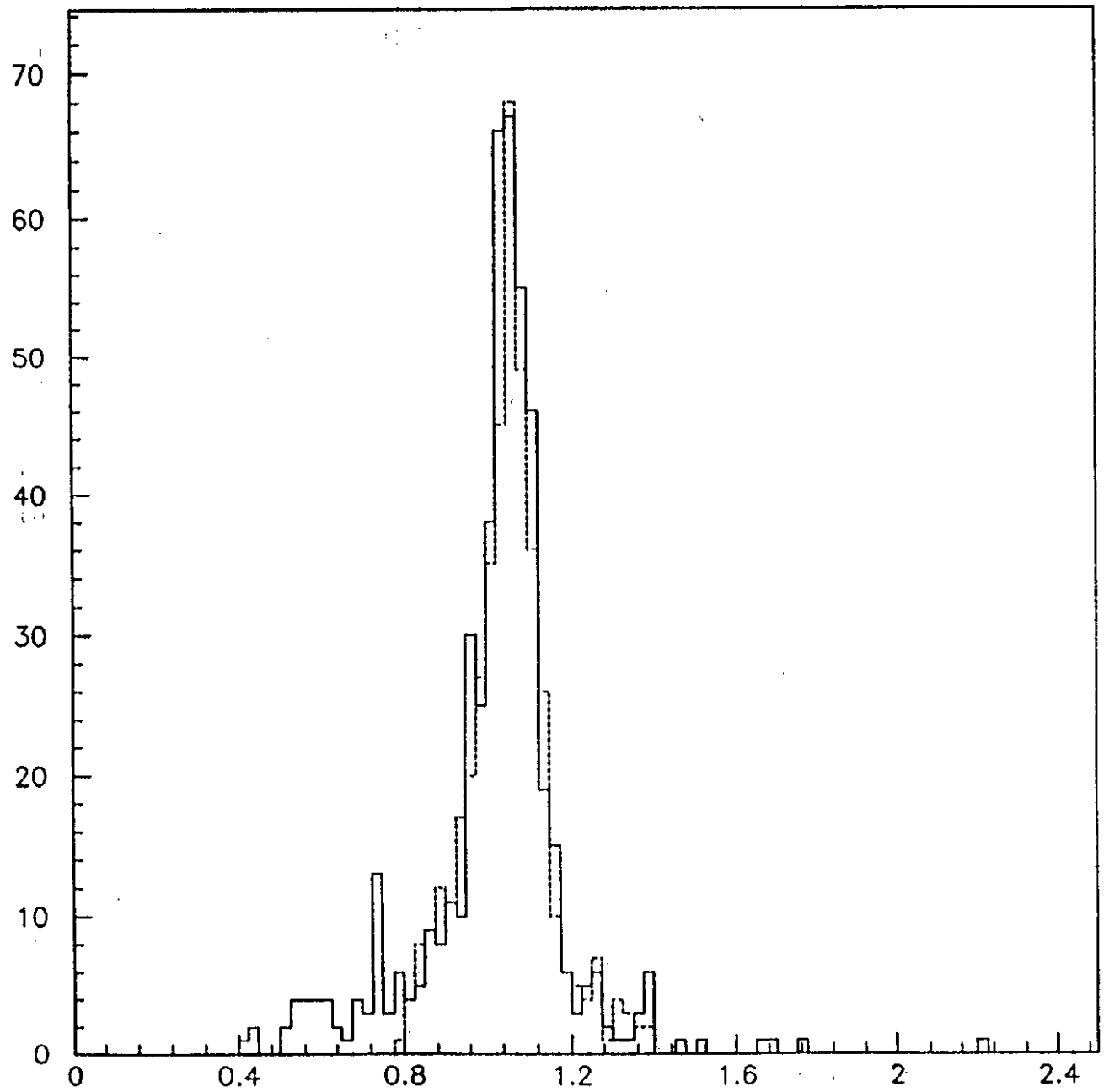

Fig.18.2 Z_550 RATIO OF RECONSTRUCTED/GENERATED MASS FOR Z0 FOR RAD=0.70

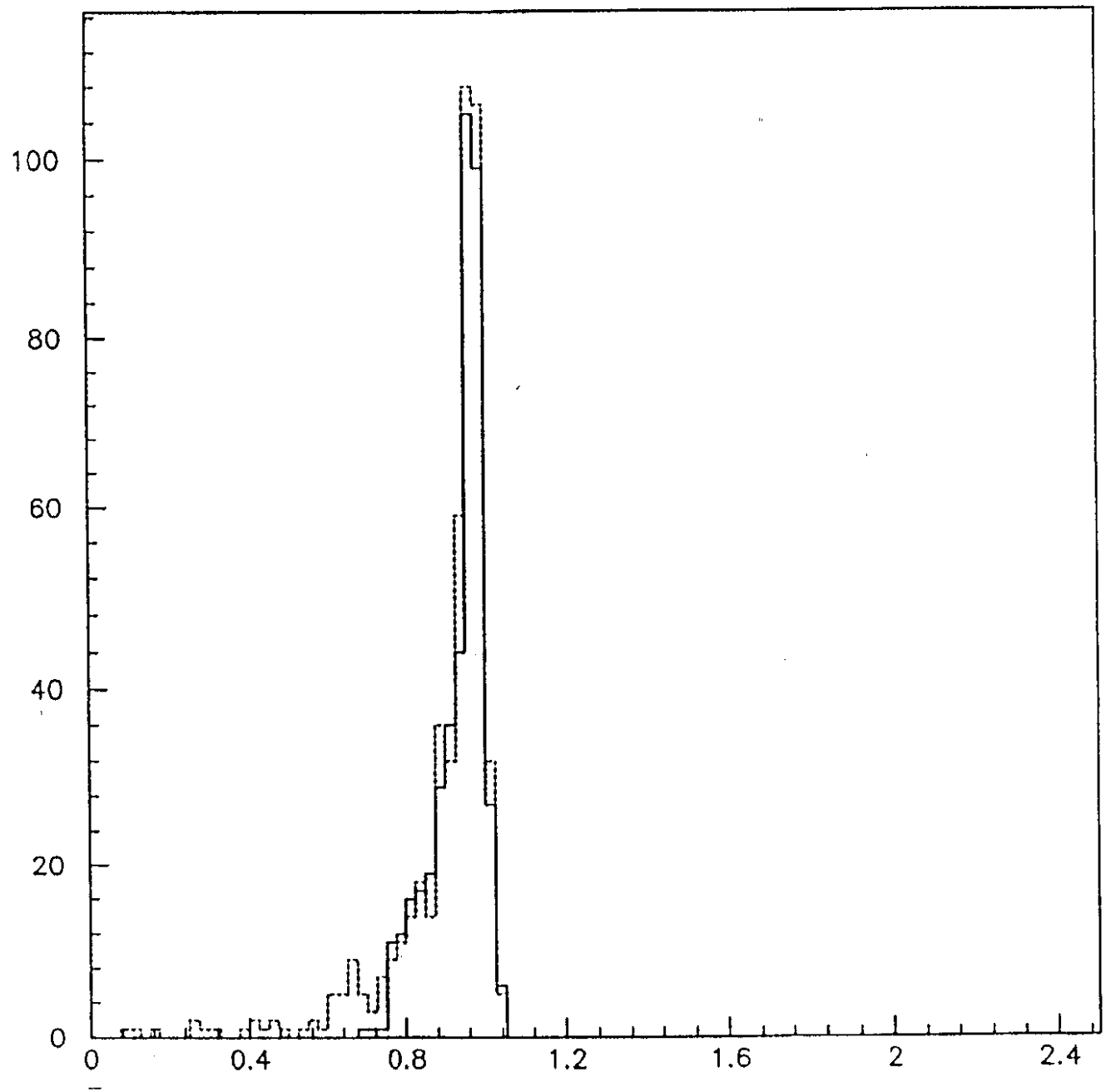

Fig.18.3 ZP_55 J–J Ratio M(rec)M(gen) clus.in Z window Z0 FOR RAD=0.70

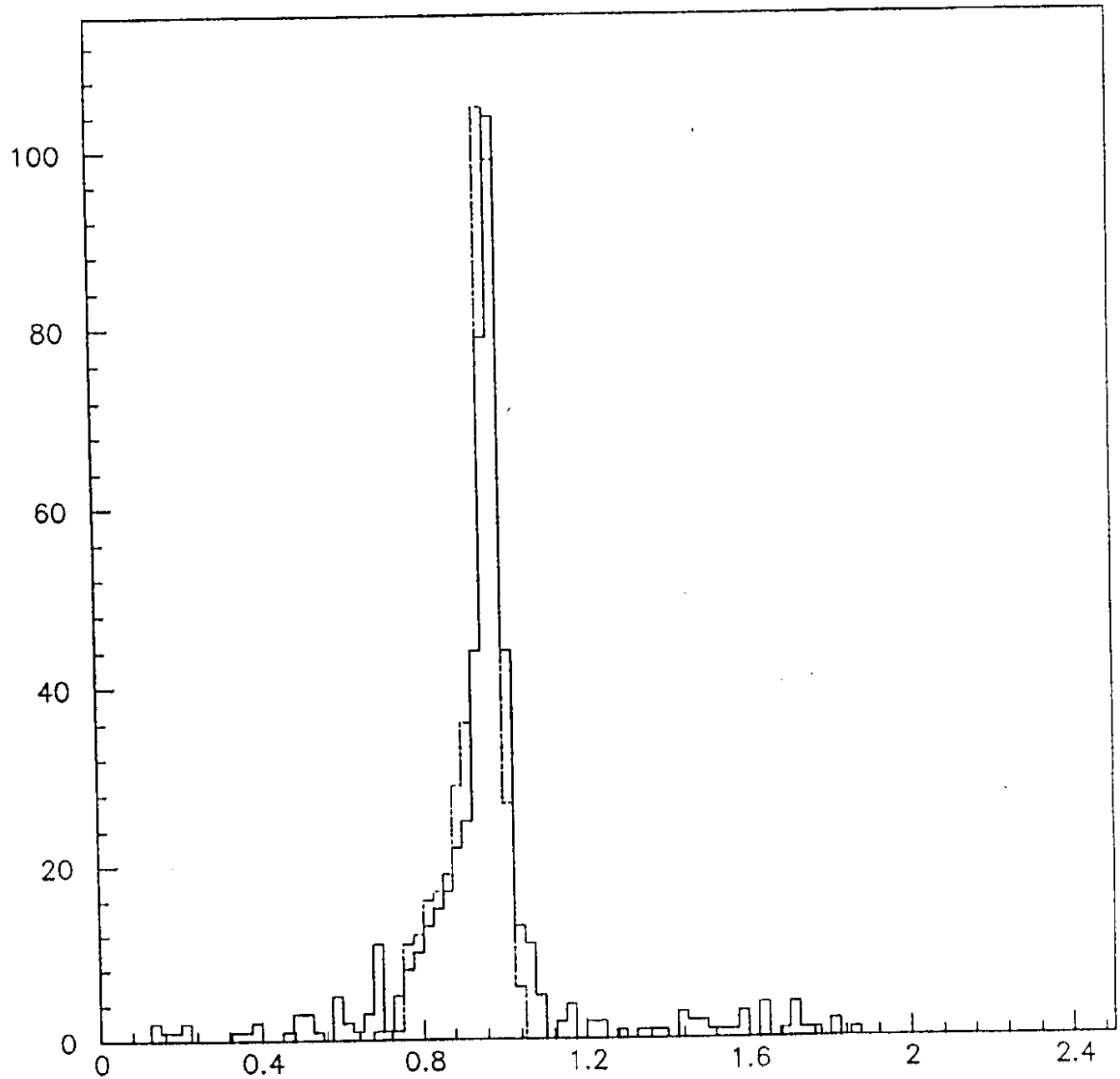

Fig.18.4 ZP_550 RATIO OF RECONSTRUCTED/GENERATED MASS FOR ZO FOR RAD=0.70

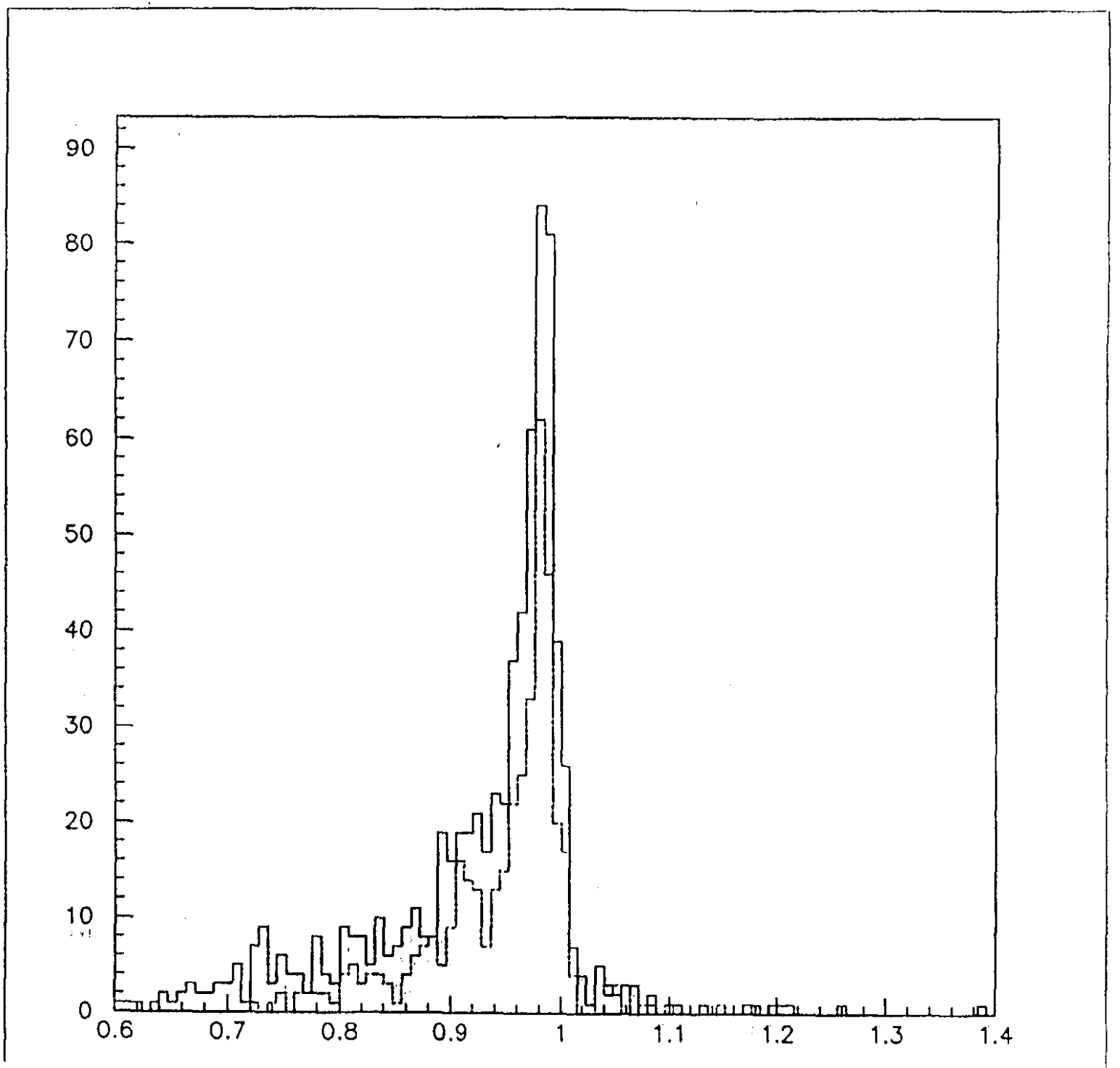

Fig.18.5 ZP_10 TeV RATIO OF RECONSTRUCTED/GENERATED MASS FOR Z0 FOR RAD=0.70

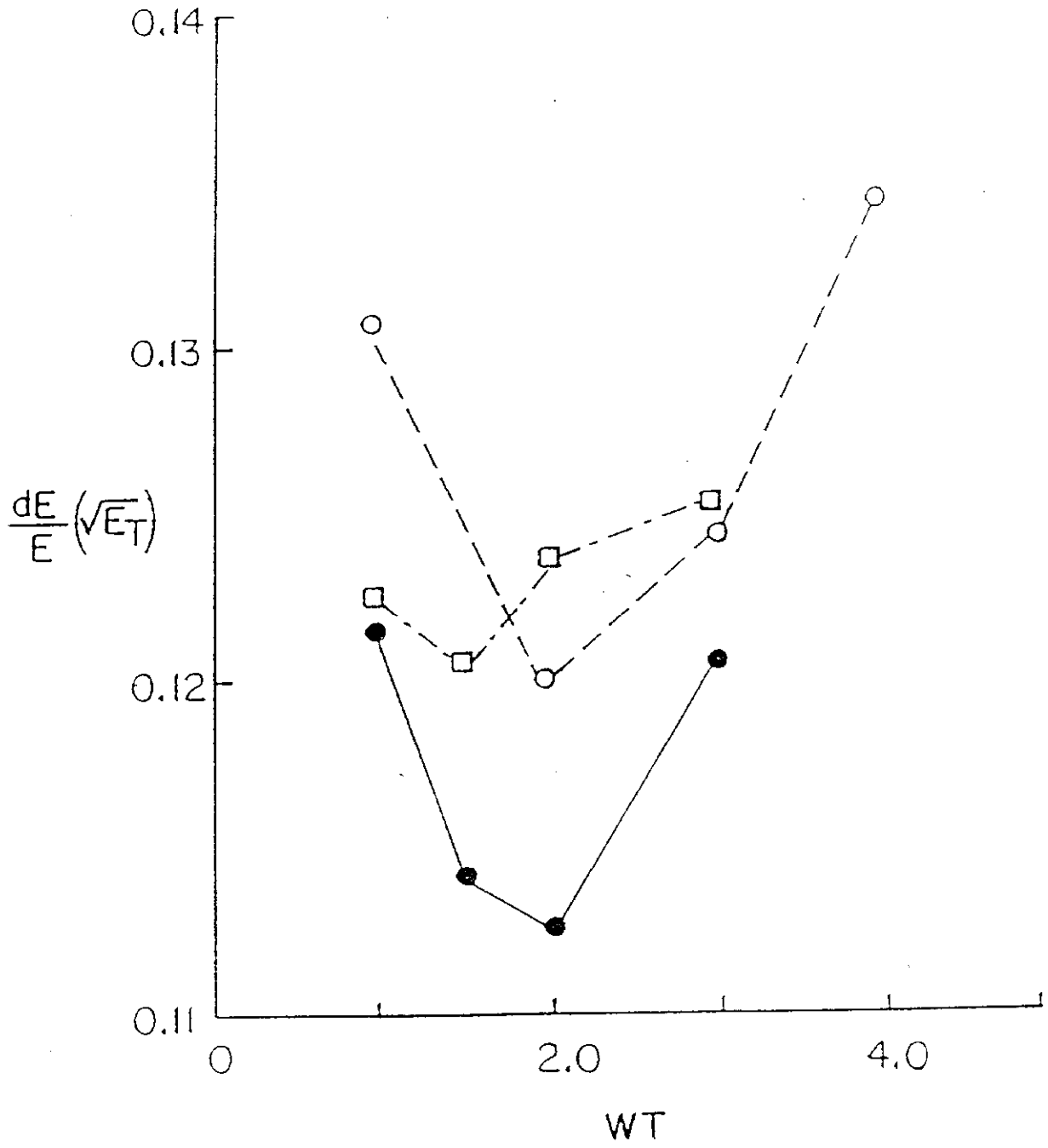

Fig. 19 Fractional energy resolution for an EM calorimeter. The results are for , °, 25 GeV, θ = 90°; , o , 25 GeV, θ = 30°; , [] , 50 GeV, θ = 90°.

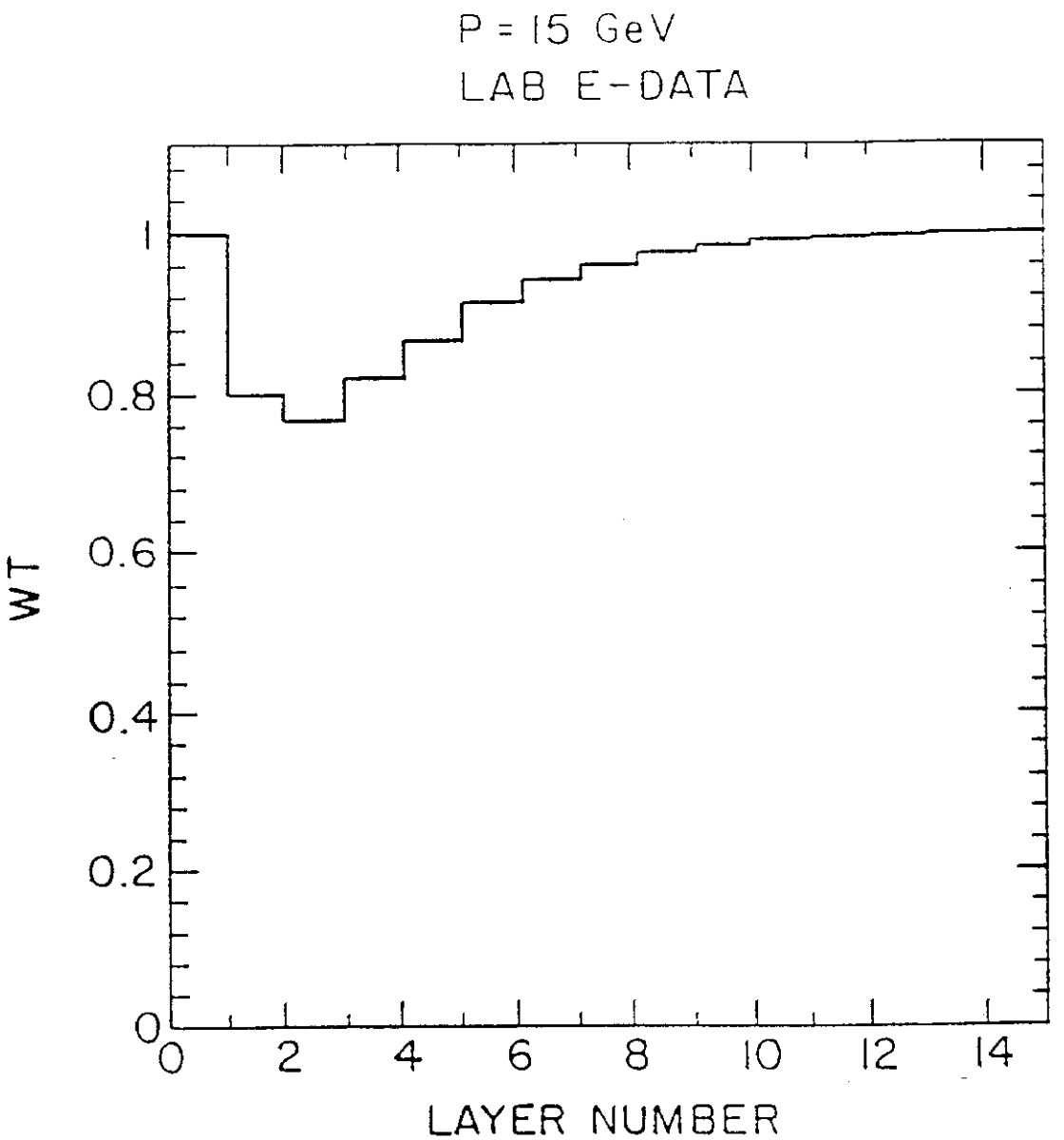

Fig.20 Weight profile in a calorimeter assuming that 15 GeV hadrons are responsible for the damage. The weight WT(z) = 1 - d(z), is plotted vs z assuming that d(z) = gf(z). The plot is for g = 1, given that the integral of f(z) is defined to be normalized to 1. A layer is $\sim$ 0.7 absorption lengths thick

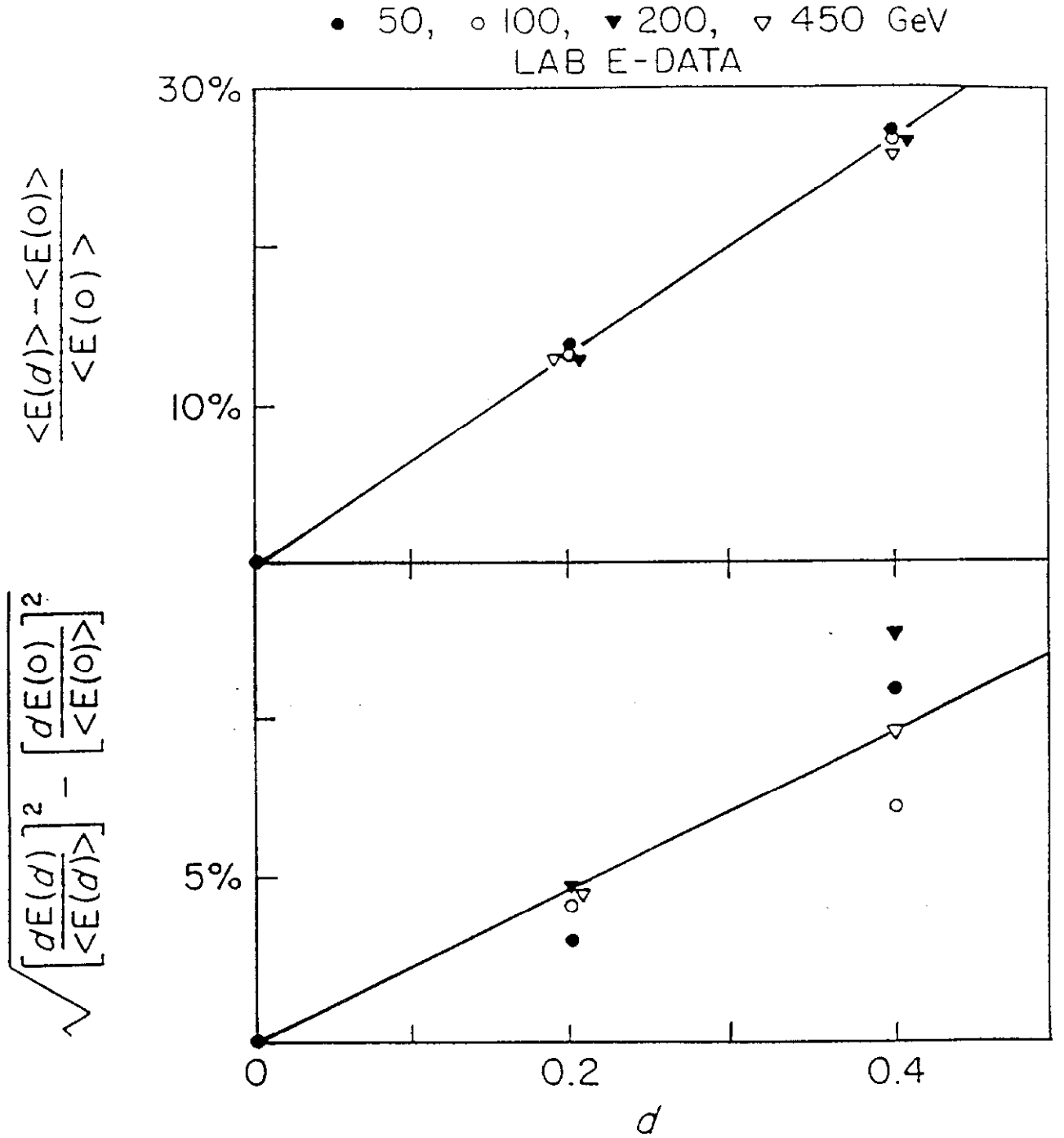

Fig.21 Mean nonlinearity and induced constant fractional energy error as a function of the peak damage $\bar{d}$ for hadrons of energy 50, •, 100 ○, 200 ▽, and 450 ▽ GeV. Both quantities appear to be roughly energy independent and linearly dependent on the peak damage coefficient, $\bar{d}$.

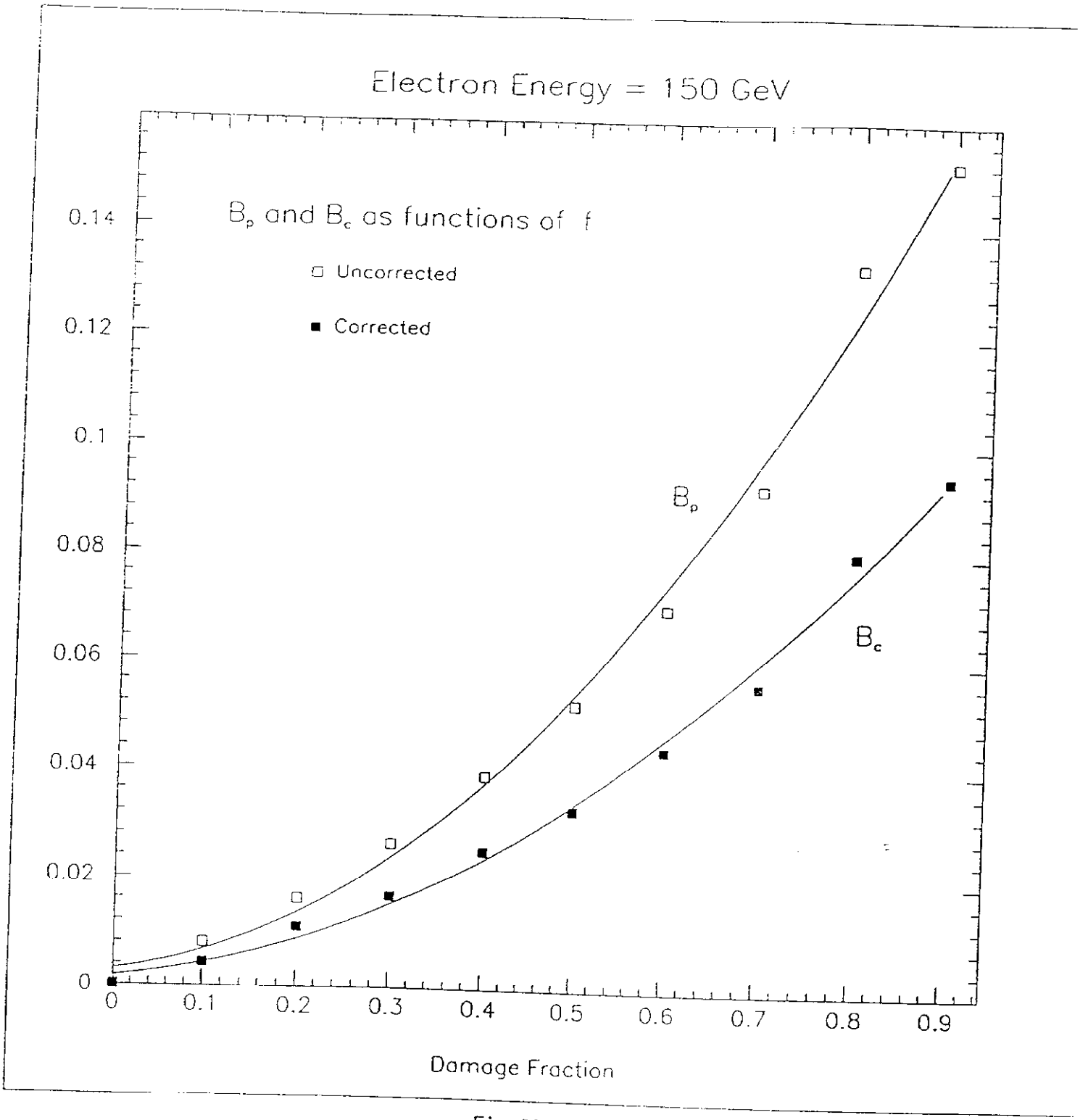

Fig.22 a)

Fig.22 The plots are uncorrected and corrected induced constant term for the EM calorimeter using the SM detector as a function of maximum damage
a) 150 GeV electrons
b) 250 GeV electrons

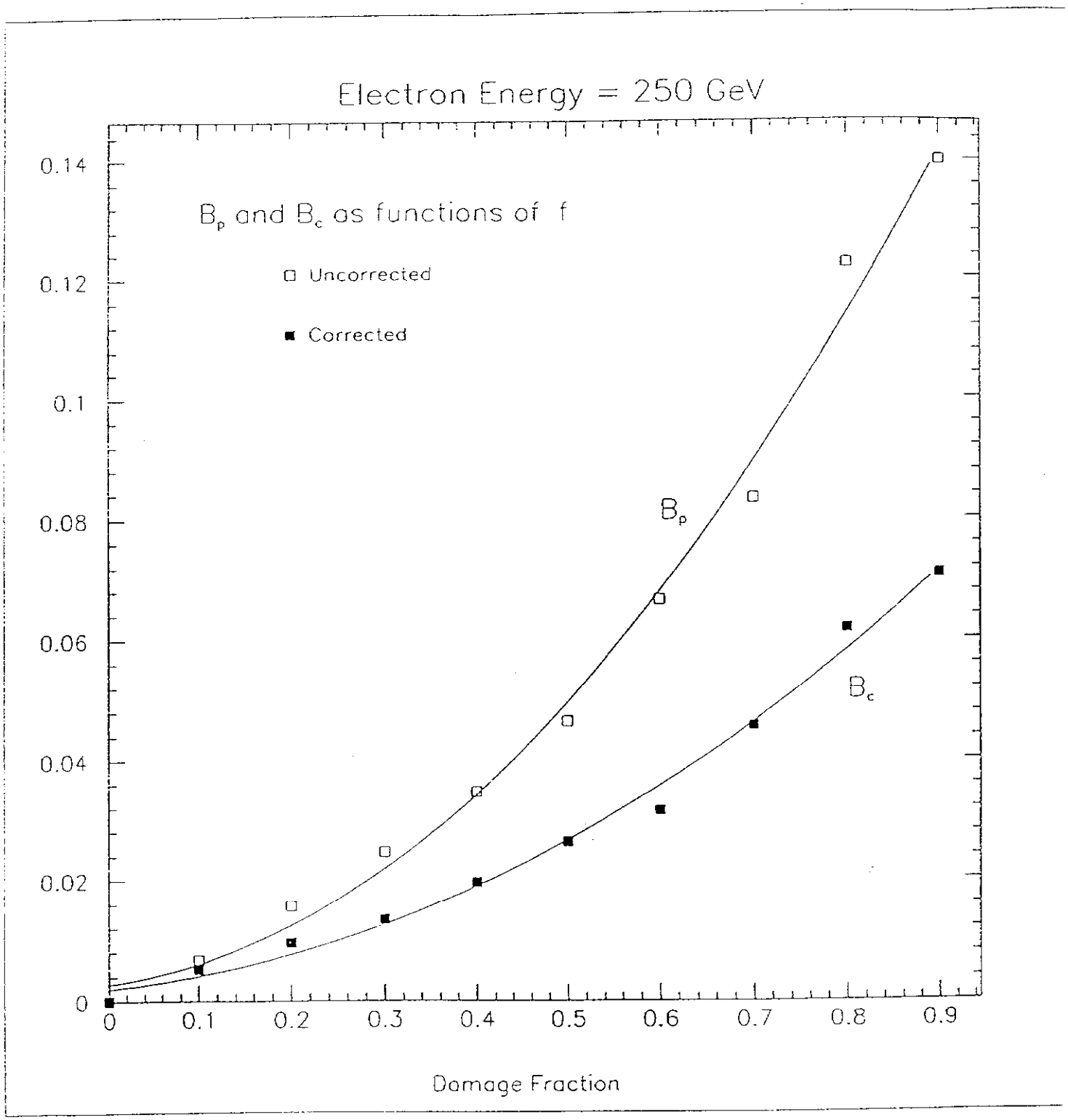
Electron Energy = 250 GeV
B_p and B_c as functions of f
Uncorrected
Corrected
B_p
B_c
0.14
0.12
0.1
0.08
0.06
0.04
0.02
0
0
0.1
0.2
0.3
0.4
0.5
0.6
0.7
0.8
0.9
Damage Fraction

Fig.22 b)